

# **Behavior of rarified steam at very high temperature**

An orientation-averaged interaction potential approach towards its  
accurate description

Ariel A. Chialvo<sup>#</sup>

Knoxville, TN 37922-3108, U. S. A.

and

Lukas Vlcek<sup>1,2</sup>

<sup>1</sup> Materials Sciences and Technology Division,  
Oak Ridge National Laboratory, Oak Ridge, TN 37831, U. S. A.

<sup>2</sup> Joint Institute for Computational Sciences  
University of Tennessee, Knoxville, Tennessee 37996, U. S. A.

Invited submission to the special issue of Molecular Physics in the occasion of the  
65<sup>th</sup> birthday of Prof. Peter T. Cummings

January 25, 2019

<sup>#</sup> To whom correspondence should be addressed ([ovlaich@gmail.com](mailto:ovlaich@gmail.com)) - ORCID # 0000-0002-6091-4563

## ABSTRACT

We propose an orientation-averaged intermolecular potential model for the accurate computation of relevant thermodynamic and transport properties of steam at conditions typically encountered in extreme environments such as rocky exoplanetary atmospheres, aircraft and rocket engines, high temperature steam reforming and electrochemical reactors, as well as advanced ultra-supercritical steam power generators. We assess the reliability of the potential model to describe accurately the temperature dependence of relevant thermodynamic (e.g., residual enthalpy, residual Gibbs free energy, residual isobaric heat capacity and speed of sound) and transport (e.g., low-density self-diffusion, shear viscosity, and thermal conductivity) properties of rarified steam up to and beyond 3000K. Moreover, we discuss some fundamental issues including: the conditions at which an orientation-averaged intermolecular potential for a molecular fluid becomes an accurate representation of the fluid behavior in extreme environments, the temperature range of validity of the approximations underlying an orientation averaging approach, and the methodology of force-field parameterization to obtain an optimized representation, as well as the concomitant modeling of the thermodynamics and transport properties of rarified fluids. Finally, we illustrate how the simultaneous accurate description of the temperature dependence of the fluid's collision integrals and second virial coefficient is crucial to the successful modeling of rarified steam in extreme environments.

## 1. INTRODUCTION

For more than two decades we have invested a great deal of effort in the interpretation of the atomistic behavior of water and aqueous solutions, from normal {Chialvo, 1994 #1246} to ultra-supercritical, {Chialvo, 2010 #7360} through near- and supercritical conditions. {Chialvo, 1999 #12518;Chialvo, 2014 #13685} The driving force underlying the effort was primarily the need for molecular-based tools able to aid the interpretation of the microstructural features of water coming from the newest and controversial (at that time) neutron diffraction with isotopic substitution — later dubbed NDIS-93 {Chialvo, 1998 #1543} — experimental data. {Chialvo, 1996 #1357;Chialvo, 2000 #1884} Because the undertaking involved mostly the analysis of liquid-like aqueous systems characterized by highly polarizable environments, it was crucial to

describe accurately the multi-body nature of water interactions, through realistic and physically meaningful polarizable intermolecular models. {Chialvo, 1996 #1423} This modeling effort culminated with the formulation of a very successful Gaussian charge polarizable model (GCPM) approach for water and aqueous solutions, {Chialvo, 1998 #1572;Paricaud, 2005 #3413;Chialvo, 2015 #14233} one that was able to describe properly the behavior of water not only for the bulk gas-phase {Benjamin, 2007 #4447} and the gas-liquid interfaces, {Rivera, 2006 #6587} but also for the condensed phases over wide ranges of environmental state conditions, *i.e.*, from the isolated dimer {Paricaud, 2005 #3413;Kiss, 2009 #6406} to extremely high temperatures and pressures, {Chialvo, 2010 #7360} though the metastable supersaturated steam phases. {Moucka, 2016 #14744}

There is however a large number of aqueous systems characterized by rather low density or dilute environments, including those in supercritical water oxidation reactors, {Yesodharan, 2002 #8084;Chialvo, 2007 #4520;Marrone, 2013 #11276;Kallikragas, 2017 #15497} ultra-supercritical steam power generators, {Moore, 2005 #5371;Viswanathan, 2005 #4485;Chialvo, 2010 #6667;Holcomb, 2014 #15516;Yeo, 2014 #15965} steam reforming reactors, {Hafizi, 2016 #15517;Solsvik, 2016 #15966} high temperature steam electrochemical reactors, {Shin, 2007 #15518;Sapountzi, 2017 #15968} geothermal systems, {Thiery, 2009 #6453;Kaasalainen, 2012 #15524;Fegley, 2016 #15970} combustion gases from conventional turbines and rocket engines {Lanzafame, 2006 #15525;Bennmansour, 2016 #15972;Xue, 2016 #15973} as well as from newer generations of propulsion systems {Ingenito, 2004 #15526;Ghassemi, 2013 #15975;Bergthorson, 2017 #15976} whose understanding — aimed at their manipulation, control, and modeling — demands a proper knowledge of steam thermophysical properties at significantly more extreme conditions than those able to be handled by equations of state. {Wagner, 2002 #3280;Haar, 1984 #1280}

A common practice in this context, as a rule of thumb in the prediction of steam properties at higher temperatures, has been either the *ad hoc* extrapolation of the thermophysical properties of steam beyond the original intended range of applications, or the extension of the range of validity of the ideal gas behavior, an approach that becomes unreliable and progressively more inaccurate with increasing pressure. {Bücker, 2003 #15515} While the behavior of steam can in principle be analyzed by atomistic simulation of realistic polarizable models, {Dang, 1997 #3939;Chialvo, 1999 #12518;Paricaud, 2005 #3413;Rivera, 2006

#6587; Yoshida, 2006 #3683; Yoshida, 2007 #3924; Kiss, 2013 #12627; Moučka, 2016 #14744} there are instances such as those where polarization effects and angular correlations become less significant portions of the system properties, when the use of atomistic models is rather inconvenient in that polarization becomes a perturbation contribution to the actual properties of steam. Such scenarios are more appropriate for perturbation approaches for anisotropic fluid interactions and less expensive than full-fledged molecular-based simulation of polarizable models. However, the reliability of the resulting perturbation expansions and the validity of the underlying approximations must be assessed by a direct comparison against the corresponding molecular simulation counterparts. {Gray, 1985 #891}

This scenario highlights the crucial need of accurate molecular-based generated thermophysical properties of rarified steam including the temperature dependence of the second virial coefficient, enthalpy, isobaric heat capacity, shear viscosity, thermal conductivity, and self-diffusion over a wide ranges of temperature typically found in rocky exoplanet atmospheres, highly energetic combustion environments such as in conventional aircraft turbines and rocket engines, newer propulsion and power generators based on metal-steam combustion, as well as the extreme environments in advanced ultra-supercritical steam power generators.

The goal of this effort is to find answers to some relevant questions including (*i*) under what conditions an orientation-averaged intermolecular potential for a molecular fluid might be an accurate representation of the fluid behavior in extreme environments?, (*ii*) how do we assess the validity of the approximations underlying an orientation averaging approach?, and (*iii*) how should we parameterize the resulting isotropic model to be able to describe accurately other fluid properties of interest?, as well as to address some emerging issues regarding the concomitant modeling of the thermodynamics and transport properties of rarified fluids.

For that purpose, we provide some relevant background information in §1, and discuss the foundations of the methodology underlying the orientation-averaged intermolecular potentials in §2. We place particular emphasis on fluids characterized by anisotropic dipolar-dipolar and dipolar-induced dipolar interactions, whose resulting orientation-averaged counterparts will be mapped onto alternative effective isotropic potential models with temperature-dependent parameters. Then, in §3 we discuss the parameterization of the resulting isotropic potential for steam based on accurate zero-density shear viscosity (or second virial

coefficient) following a recently proposed optimization approach based on the statistical distance minimization. {Vlcek, 2015 #14597} The resulting parameterization is finally applied to the prediction of the second virial coefficient (or zero-density shear viscosity), enthalpy, isobaric heat capacity, as well as the **zero-pressure self-diffusion and thermal conductivity coefficients** of water in extremely high temperature environments. Finally, we close the manuscript with a brief discussion of relevant emerging issues and future outlook.

## 2. ORIENTATION-AVERAGED INTERACTION POTENTIALS FOR RARIFIED STEAM

### a *Rationale and fundamentals*

The rationale behind the use of orientation-averaged potentials is the need to simplify the calculation of the properties of fluids characterized by anisotropic interactions in terms of their isotropic counterparts for which we already have reliable methodologies. {Gray, 1985 #891} While the most obvious method involves the orientational (canonical ensemble) average of the interaction potential itself, *i.e.*, {Bae, 1967 #15068}

$$\langle \phi(r) \rangle_{\omega}^{canon} = \int \phi_{12}(\mathbf{r}, \boldsymbol{\omega}) e^{-\beta \phi_{12}(\mathbf{r}, \boldsymbol{\omega})} d\boldsymbol{\omega} / \int e^{-\beta \phi_{12}(\mathbf{r}, \boldsymbol{\omega})} d\boldsymbol{\omega} \quad (1)$$

over the phase space generated by the interaction model representing the fluid — where

$\beta = (kT)^{-1}$  while  $\phi_{12}(\mathbf{r}, \boldsymbol{\omega})$  is the interaction potential between molecules 1 and 2, located by the vector positions  $\mathbf{r}_1$  and  $\mathbf{r}_2$ , and space orientations  $\boldsymbol{\omega}_1$  and  $\boldsymbol{\omega}_2$  — yet, the most advantageous averaging approach would be the one that also reproduces the correct configurational partition function of the system, *i.e.*, its free energy, and consequently, its microstructure and either configurational or residual thermodynamic properties.

The underlying idea hinges around the mapping of the configurational partition function  $\mathcal{Z}$  for the interaction of a pair of anisotropic (*e.g.*, polar) molecules onto the corresponding to an unweighted orientation-averaged configurational integrand, *i.e.*,

$$\mathcal{Z} = \Omega^{-2} \int e^{-\beta \phi_{12}(\mathbf{r}, \boldsymbol{\omega})} d\mathbf{r}_1 d\mathbf{r}_2 d\boldsymbol{\omega}_1 d\boldsymbol{\omega}_2 \rightarrow \int \langle e^{-\beta \phi_{12}(\mathbf{r}, \boldsymbol{\omega})} \rangle_{\omega} d\mathbf{r}_1 d\mathbf{r}_2 \quad (2)$$

Consequently, the un-weighted orientation-average  $\langle \cdots \rangle_{\omega} \neq \langle \cdots \rangle_{\omega}^{canon}$  is given by the following orientation-averaged integrand,

$$\left\langle e^{-\beta\phi_{12}(\mathbf{r}, \boldsymbol{\omega})} \right\rangle_{\boldsymbol{\omega}} = \Omega^{-2} \int e^{-\beta\phi_{12}(\mathbf{r}, \boldsymbol{\omega})} d\boldsymbol{\omega}_1 d\boldsymbol{\omega}_2 \quad (3)$$

*i.e.*, also known as the reference average Mayer function, {Perram, 1974 #15510} where  $\Omega_i = \int d\boldsymbol{\omega}_i$  is the phase space integral over the angular orientation of the  $i$ -molecule, with either  $d\boldsymbol{\omega}_i = \sin\theta_i d\theta_i d\varphi_i$  and  $\Omega = 4\pi$  for linear molecules or  $d\boldsymbol{\omega}_i = \sin\theta_i d\theta_i d\varphi_i d\psi_i$  and  $8\pi^2$  for non-linear molecules. {Gray, 1985 #891} For the case under consideration, *i.e.*, axially symmetric molecules (see Figure A1), Eqns. (2)-(3) can be rewritten in terms of relative coordinates,  $\mathbf{r}_{12} = \mathbf{r}_1 - \mathbf{r}_2$  and  $\varphi_{12} = \varphi_1 - \varphi_2$ , as follows,

$$\mathcal{Z} = V \int \left\langle e^{-\beta\phi_{12}(\mathbf{r}, \boldsymbol{\omega})} \right\rangle_{\boldsymbol{\omega}} d\mathbf{r}_{12} \quad (4)$$

where  $d\mathbf{r}_1 d\mathbf{r}_2 = d\mathbf{r}_1 d\mathbf{r}_{12}$  and  $V = \int d\mathbf{r}_1$  with,

$$\begin{aligned} \left\langle e^{-\beta\phi_{12}(\mathbf{r}, \boldsymbol{\omega})} \right\rangle_{\boldsymbol{\omega}} &= (4\pi)^{-2} \int d\boldsymbol{\omega}_1 \int e^{-\beta\phi_{12}(\mathbf{r}, \boldsymbol{\omega})} d\boldsymbol{\omega}_{12} \\ &= (8\pi)^{-1} \int e^{-\beta\phi_{12}(\mathbf{r}, \boldsymbol{\omega})} d\boldsymbol{\omega}_{12} \end{aligned} \quad (5)$$

after invoking  $d\boldsymbol{\omega}_1 d\boldsymbol{\omega}_{12} = \sin\theta_1 d\theta_1 \sin\theta_2 d\theta_2 d\varphi_1 d\varphi_{12}$  and  $\int d\varphi_1 = 2\pi$ . Therefore, we can define an orientation-averaged interaction potential  $\Phi_{12}(r)$  making possible to express Eqn. (4) in the following alternative form,

$$\mathcal{Z} = V \int e^{-\beta\Phi_{12}(r)} d\mathbf{r}_{12} \quad (6)$$

Moreover, after invoking Eqn. (5), we can make identify the explicit link between the original orientation-dependent interaction potential  $\phi_{12}(\mathbf{r}, \boldsymbol{\omega})$  and the (free energy) orientation-averaged potential  $\Phi_{12}(\mathbf{r})$ , *i.e.*, {Danon, 1969 #15509}

$$\begin{aligned} \Phi_{12}(r) &= -kT \ln \left\langle e^{-\beta\phi_{12}(\mathbf{r}, \boldsymbol{\omega})} \right\rangle_{\boldsymbol{\omega}} \\ &= -kT \ln \left[ (8\pi)^{-1} \int e^{-\beta\phi_{12}(\mathbf{r}, \boldsymbol{\omega})} d\boldsymbol{\omega}_{12} \right] \end{aligned} \quad (7)$$

An important issue here regards the link between the isotropic potentials  $\langle \phi(r) \rangle_{\omega}^{canon}$  defined by Eqn. (1), and  $\Phi_{12}(r)$  described by Eqn. (7), as well as the advantages/shortcomings of using one over the other. Note that we can rewrite Eqn. (1) as follows,

$$\begin{aligned}\langle \phi(r) \rangle_{\omega}^{canon} &= \frac{\int \phi_{12}(\mathbf{r}, \boldsymbol{\omega}) e^{-\beta \phi_{12}(\mathbf{r}, \boldsymbol{\omega})} d\boldsymbol{\omega} / \int d\boldsymbol{\omega}}{\int e^{-\beta \phi_{12}(\mathbf{r}, \boldsymbol{\omega})} d\boldsymbol{\omega} / \int d\boldsymbol{\omega}} \\ &= \frac{\langle \phi_{12}(\mathbf{r}, \boldsymbol{\omega}) e^{-\beta \phi_{12}(\mathbf{r}, \boldsymbol{\omega})} \rangle_{\omega}}{\langle e^{-\beta \phi_{12}(\mathbf{r}, \boldsymbol{\omega})} \rangle_{\omega}}\end{aligned}\quad (8)$$

while Eqn. (7) provides a way to determine the following temperature derivative,

$$\begin{aligned}\left( \frac{d\Phi_{12}(r)}{d\beta} \right)_r &= \beta^{-2} \ln \left\langle e^{-\beta \phi_{12}(\mathbf{r}, \boldsymbol{\omega})} \right\rangle_{\omega} + \\ &\quad \beta^{-1} \int \phi_{12}(\mathbf{r}, \boldsymbol{\omega}) e^{-\beta \phi_{12}(\mathbf{r}, \boldsymbol{\omega})} d\boldsymbol{\omega} / \int e^{-\beta \phi_{12}(\mathbf{r}, \boldsymbol{\omega})} d\boldsymbol{\omega}\end{aligned}\quad (9)$$

After identifying the first term of Eqn. (9) as  $\beta^{-1} \Phi_{12}(r)$  according to Eqn. (7), and the second term as  $\beta^{-1} \langle \phi(r) \rangle_{\omega}^{canon}$  according to Eqn. (8), the formal link between the canonical and the free energy-based orientation averages of the original anisotropic potential  $\phi_{12}(\mathbf{r}, \boldsymbol{\omega})$  becomes,

$$\langle \phi(r) \rangle_{\omega}^{canon} = \Phi_{12}(r) + \beta \left( \frac{d\Phi_{12}(r)}{d\beta} \right)_r \quad (10)$$

While Eqn. (10) embodies a statistical mechanical identity — representing the microscopic manifestation of the thermodynamic relation between the configurational energy and its configurational free energy counterpart {Rushbrooke, 1940 #15519} — for all practical purposes it becomes more advantageous to expand the exponentials within each  $\langle \dots \rangle_{\omega}$  of Eqn. (8) as truncated perturbation series, *i.e.*,

$$\begin{aligned}\langle \phi_{12}(\mathbf{r}, \boldsymbol{\omega}) e^{-\beta \phi_{12}(\mathbf{r}, \boldsymbol{\omega})} \rangle_{\omega} &= \langle \phi_{12}(\mathbf{r}, \boldsymbol{\omega}) [1 - \beta \phi_{12}(\mathbf{r}, \boldsymbol{\omega}) + \beta^2 \phi_{12}^2(\mathbf{r}, \boldsymbol{\omega})/2 - \\ &\quad \beta^3 \phi_{12}^3(\mathbf{r}, \boldsymbol{\omega})/6 + \dots] \rangle_{\omega} \\ &= \langle \phi_{12}(\mathbf{r}, \boldsymbol{\omega}) \rangle_{\omega} - \beta \langle \phi_{12}^2(\mathbf{r}, \boldsymbol{\omega}) \rangle_{\omega} + (\beta^2/2) \langle \phi_{12}^3(\mathbf{r}, \boldsymbol{\omega}) \rangle_{\omega} - \\ &\quad (\beta^3/6) \langle \phi_{12}^4(\mathbf{r}, \boldsymbol{\omega}) \rangle_{\omega} + \dots\end{aligned}\quad (11)$$

for the numerator and,

$$\begin{aligned}\langle e^{-\beta\phi_{12}(\mathbf{r},\boldsymbol{\omega})} \rangle_\omega &= \langle 1 - \beta\phi_{12}(\mathbf{r},\boldsymbol{\omega}) + \beta^2\phi_{12}^2(\mathbf{r},\boldsymbol{\omega})/2 - \beta^3\phi_{12}^3(\mathbf{r},\boldsymbol{\omega})/6 + \dots \rangle_\omega \\ &= 1 - \beta\langle\phi_{12}(\mathbf{r},\boldsymbol{\omega})\rangle_\omega + (\beta^2/2)\langle\phi_{12}^2(\mathbf{r},\boldsymbol{\omega})\rangle_\omega - \\ &\quad (\beta^3/6)\langle\phi_{12}^3(\mathbf{r},\boldsymbol{\omega})\rangle_\omega + \dots\end{aligned}\quad (12)$$

for the denominator of Eqn. (8), respectively. Moreover, whenever the expression

$\ln(1-x+x^2/2-x^3/6+\dots) \approx -x+x^2/2-x^3/6+\dots$  is an accurate approximation, Eqns. (7) and

(12) lead to the following truncated perturbation expansions,

$$\begin{aligned}\Phi_{12}(r) &= \langle\phi_{12}(\mathbf{r},\boldsymbol{\omega})\rangle_\omega - (\beta/2)\langle\phi_{12}^2(\mathbf{r},\boldsymbol{\omega})\rangle_\omega + (\beta^2/6)\langle\phi_{12}^3(\mathbf{r},\boldsymbol{\omega})\rangle_\omega - \\ &\quad (\beta^3/24)\langle\phi_{12}^4(\mathbf{r},\boldsymbol{\omega})\rangle_\omega - \dots\end{aligned}\quad (13)$$

$$\begin{aligned}(d\Phi_{12}(r)/d\beta)_r &= -(1/2)\langle\phi_{12}^2(\mathbf{r},\boldsymbol{\omega})\rangle_\omega + (\beta/3)\langle\phi_{12}^3(\mathbf{r},\boldsymbol{\omega})\rangle_\omega - \\ &\quad (\beta^2/8)\langle\phi_{12}^4(\mathbf{r},\boldsymbol{\omega})\rangle_\omega - \dots\end{aligned}\quad (14)$$

since  $\langle\phi_{12}(\mathbf{r},\boldsymbol{\omega})\rangle_\omega \neq f(\beta)$ . After substituting Eqns. (13)-(14) into (10) we immediately conclude that, under the state conditions where the above approximations are obeyed, the canonical orientation-averaged potential is linked to the free-energy orientation-averaged potential as follows,

$$\begin{aligned}\langle\phi(r)\rangle_\omega^{canon} &= \langle\phi_{12}(\mathbf{r},\boldsymbol{\omega})\rangle_\omega - \beta\langle\phi_{12}^2(\mathbf{r},\boldsymbol{\omega})\rangle_\omega + (\beta^2/2)\langle\phi_{12}^3(\mathbf{r},\boldsymbol{\omega})\rangle_\omega - \\ &\quad (\beta^3/6)\langle\phi_{12}^4(\mathbf{r},\boldsymbol{\omega})\rangle_\omega + \dots\end{aligned}\quad (15)$$

The two orientation-averaged potentials, Eqns. (13) and (15), share an important common feature, *i.e.*, in contrast to their original anisotropic forms, the isotropic counterparts become temperature dependent. However, the magnitude of their temperature-dependent terms are significantly different; in fact, a direct term-to-term comparison between Eqns. (13) and (15) indicates that the temperature-dependent coefficients of  $\langle\phi(r)\rangle_\omega^{canon}$  are always larger, by a factor of 2, 3, 4, and so on, than the corresponding to  $\Phi_{12}(r)$ . This feature flags the need for caution

when using these truncated expansions, in particular, first-order expressions as we will discuss and illustrate below.

Typically for a neutral polar system  $\phi_{12}(\mathbf{r}, \boldsymbol{\omega})$  can be described by a multipole expansion, {Gray, 1985 #891} whose immediate consequence is that  $\langle \phi_{12}^n(\mathbf{r}, \boldsymbol{\omega}) \rangle_\omega = 0$  for odd values of  $n$ . Moreover, from Eqns. (13) and (15) we find that,

$$\Phi_{12}(r) = -(\beta/2)\langle \phi_{12}^2(\mathbf{r}, \boldsymbol{\omega}) \rangle_\omega - (\beta^3/24)\langle \phi_{12}^4(\mathbf{r}, \boldsymbol{\omega}) \rangle_\omega + \dots \quad (16)$$

$$\langle \phi_{12}(r) \rangle_\omega^{canon} = -\beta\langle \phi_{12}^2(\mathbf{r}, \boldsymbol{\omega}) \rangle_\omega - (\beta^3/6)\langle \phi_{12}^4(\mathbf{r}, \boldsymbol{\omega}) \rangle_\omega + \dots \quad (17)$$

where the indicated orientation-averages on the right-hand-side of these equations can be straightforwardly determined from their definitions, as addressed in the next section for polar fluids.

### b Dipole-dipole and dipole-induced dipole interactions

Here we derive the orientation-averaged potentials relevant to the description of the thermophysical behavior of rarified polar fluids. For that purpose, we start with the first relevant contribution to the potential function of polar fluids, the permanent dipole-permanent dipole interactions (see Appendix A), *i.e.*,

$$\phi_{12}^{pp}(r, \boldsymbol{\omega}) = (\mu_1 \mu_2 / r_{12}^3)(\sin \theta_1 \sin \theta_2 \cos \varphi_{12} - 2 \cos \theta_1 \cos \theta_2) \quad (18)$$

for which the second-order truncated orientation-averaged dipole-dipole interaction potentials, Eqns. (16)-(17), become,

$$\Phi_{12}(r) = -(\beta/3)\mu_1^2 \mu_2^2 / r_{12}^6 - (\beta^3/25)\mu_1^4 \mu_2^4 / r_{12}^{12} + \dots \quad (19)$$

$$\langle \phi_{12}(r) \rangle_\omega^{canon} = -(2\beta/3)\mu_1^2 \mu_2^2 / r_{12}^6 - (4\beta^3/25)\mu_1^4 \mu_2^4 / r_{12}^{12} + \dots \quad (20)$$

whose full derivation is given in Appendix S1 of the supplementary information document.

The next relevant contribution to the potential function comes from the permanent dipole-induced dipole interactions (see Appendix A), *i.e.*,

$$\phi_{12}^{\mu\alpha}(r, \omega) = -[\alpha_1 \mu_2^2 (3 \cos^2 \theta_2 + 1) + \alpha_2 \mu_1^2 (3 \cos^2 \theta_1 + 1)] / 2 r_{12}^6 \quad (21)$$

so that the actual anisotropic potential comprises the interactions of permanent and induced dipoles,

$$\phi_{12}^{\mu d}(r, \omega) = \phi_{12}^{\mu\mu}(r, \omega) + \phi_{12}^{\mu\alpha}(r, \omega) = \phi_{12}(r, \omega) \quad (22)$$

whose orientation-averaged (isotropic) counterparts become (see Appendix S1 in the supplementary document),

$$\Phi_{12}(r) = -[\alpha_1 \mu_2^2 + \alpha_2 \mu_1^2 + \beta \mu_1^2 \mu_2^2 / 3] / r_{12}^6 - (\beta / 25) [\beta^2 \mu_1^4 \mu_2^4 + (144 \alpha_1 \mu_2^2 \alpha_2 \mu_1^2 - 15 \alpha_1^2 \mu_2^4 - 15 \alpha_2^2 \mu_1^4)] / r_{12}^{12} \quad (23)$$

and,

$$\langle \phi_{12}(r) \rangle_{\omega}^{\text{canon}} = -[\alpha_1 \mu_2^2 + \alpha_2 \mu_1^2 + 2 \beta \mu_1^2 \mu_2^2 / 3] / r_{12}^6 - (4 \beta / 25) [\beta^2 \mu_1^4 \mu_2^4 + (144 \alpha_1 \mu_2^2 \alpha_2 \mu_1^2 - 15 \alpha_1^2 \mu_2^4 - 15 \alpha_2^2 \mu_1^4)] / r_{12}^{12} \quad (24)$$

Note that if we added the contribution of the van der Waals interactions, as described by an isotropic Lennard-Jones potential, to the above averaged potential, *i.e.*,

$$\begin{aligned} \Psi(r) &= 4 \varepsilon_{LJ} \left[ (\sigma_{LJ}/r)^{12} - (\sigma_{LJ}/r)^6 \right] - (2 \alpha \mu^2 + f \beta \mu^4 / 3) / r^6 - \\ &\quad (f^2 \beta / 25) (\beta^2 \mu^8 + 114 \alpha^2 \mu^4) / r^{12} \quad (25) \\ &= 4 \varepsilon_{eff} \left[ (\sigma_{eff}/r)^{12} - (\sigma_{eff}/r)^6 \right] \end{aligned}$$

and — where for notational simplicity sake we assume a one-component fluid, with  $f = 1$  for the free energy orientation-averaged potential, Eqn. (23), and  $f = 2$  for the canonical orientation-averaged potential, Eqn. (24) — we will be able to define an effective Lennard-Jones potential, last line of Eqn. (25). This effective potential comprises obviously temperature-dependent force-field parameters. In fact, the effective parameters can be related to the original Lennard-Jones parameters through the following scaling functions,

$$\mathcal{S}(T) = 1 + (6\alpha\mu^2 + f\beta\mu^4)/(12\varepsilon_{LJ}\sigma_{LJ}^6) \quad (26)$$

with,

$$\begin{aligned}\varepsilon_{eff}(T) &= \varepsilon_{LJ}\mathcal{S}^2(T) \\ \sigma_{eff}(T) &= \sigma_{LJ}\mathcal{S}^{-1/6}(T)\end{aligned}\quad (27)$$

when including the first non-vanishing terms of Eqns. (13) and (15) in Eqn. (25). Likewise,

$$\mathcal{S}_1(T) = 1 - f^2(114\beta\alpha^2\mu^4 + \beta^3\mu^8)/(100\varepsilon_{LJ}\sigma_{LJ}^{12}) \quad (28)$$

$$\mathcal{S}_2(T) = 1 + (2\alpha\mu^2 + f\beta\mu^4/3)/(4\varepsilon_{LJ}\sigma_{LJ}^6) \quad (29)$$

so that,

$$\begin{aligned}\varepsilon_{eff}(T) &= \varepsilon_{LJ}\mathcal{S}_2^2(T)/\mathcal{S}_1(T) \\ \sigma_{eff}(T) &= \sigma_{LJ}[\mathcal{S}_1(T)/\mathcal{S}_2(T)]^{1/6}\end{aligned}\quad (30)$$

when including first and second non-vanishing terms. The link between the two lines in Eqns. (27) and (30) can straightforwardly be proved by their substitution into the bottom line of Eqn. (25).

For the sake of completeness, we note that the formalism applies equally when one of the molecules in the pair interaction is either non-polar, non-polarizable or both. For example, if species 2 in Eqn. (23) is non-polar but polarizable, *i.e.*,  $\mu_2 = 0$  and  $\alpha_2 \neq 0$ , then

$$\Phi_{12}(r) = -\alpha_2\mu_1^2/r_{12}^6 + 3f^2\beta\alpha_2^2\mu_1^4/5r_{12}^{12} \quad (31)$$

so that  $\mathcal{S}_1(T) = 1 + 3f^2\beta\alpha_2^2\mu_1^4/(20\varepsilon_{LJ}\sigma_{LJ}^{12})$ ,  $\mathcal{S}_2(T) = 1 + f\beta\alpha_2\mu_1/(4\varepsilon_{LJ}\sigma_{LJ}^6)$ , and consequently,

we have again an effective Lennard-Jones potential characterized by  $\varepsilon_{eff}(T) = \varepsilon_{LJ}\mathcal{S}_2^2(T)/\mathcal{S}_1(T)$

and  $\sigma_{eff}(T) = \sigma_{LJ}[\mathcal{S}_1(T)/\mathcal{S}_2(T)]^{1/6}$ .

### c Comparison between actual anisotropic and resulting orientation-averaged potentials

As a matter of illustration, and to highlight the limitations of the resulting orientation-averaged potentials, here we analyze the temperature dependence of the second virial coefficient of a polarizable Stockmayer fluid against those from the resulting two effective Lennard-Jones fluid approximations, *i.e.*, Eqn. (25) with either  $f = 1$  or  $f = 2$ . Under the polarizable Stockmayer label here we also identify the model defined as the first order  $\alpha$ -perturbation expansion of the self-consistent induced-dipole polarization contribution as described in Appendix A. {Buckingham, 1955 #15511} Because the first order  $\alpha$ -perturbation expansion model provides essentially identical orientation-averaged pair potentials to those from the self-consistent polarizable Stockmayer model as illustrated in Figure A3, in what follows we study the behavior of the first-order  $\alpha$ -perturbation expansion model.

For that purpose the interaction potential model, aimed at describing a low-density steam-like vapor, is defined by the original non-polarizable Stockmayer {Maitland, 1981 #370} plus the dipole-induced dipole contributions, Eqn. (22) above, and characterized by the Lennard-Jones parameters  $\varepsilon_{LJ} = 283.7k(K)$  and  $\sigma_{LJ} = 2.920\text{\AA}$  as well as the molecular polarizability  $\alpha = 1.444\text{\AA}^3$  and the permanent dipole moment  $\mu = 1.855D$ .

In Figure 1 we display the temperature dependence for the second virial coefficient of the polarizable Stockmayer anisotropic model fluid, determined by the methodology described in Appendix S2 (supplementary information document), in comparison with the corresponding isotropic free energy orientation-averaged and canonical orientation-averaged potential counterparts as described by Eqn. (27) with  $f = 1$  and  $f = 2$ , respectively. The comparison also comprises the adjusted canonical orientation-averaged potential proposed by Paul and Warnatz {Paul, 1998 #15512} with the adjustment parameter  $\gamma = 0.25$  in their notation, *i.e.*, for which  $f \equiv 2\gamma = 0.5$  according to our notation.

Figure 1 highlights a few important features of the orientation-averaged representations for the second virial coefficient of the original anisotropic model fluid, namely: (a) they exhibit rather contrasting temperature dependence translating into significant deviations from the actual behavior; (b) they are a manifestation of the approximations underlying the expansion of the Boltzmann factor, Eqns. (11)-(12), and subsequently, their logarithms; (c) not surprisingly, the free energy orientation-averaged model shows the most accurate prescription for the isotropic representation over a wider range of temperature, *i.e.*, it reproduces more closely the correct

Ariel Chialvo 4/28/2017 2:58 PM  
Comment [1]:

Ariel Chialvo 5/22/2017 10:43 AM  
Comment [2]:

configurational partition function of the anisotropic fluid; and (d) the  $\gamma = 0.25$  adjustment parameter introduced by Paul and Warnatz {Paul, 1998 #15512} to correct the actual canonical orientation-averaged potential obviously improves it, but it fails in comparison with the free energy-based representation. In other words, these features indicate that (*i*) the free energy orientation-averaged representation becomes increasingly less accurate, say, with a relative deviation of  $\sim 9\%$  for  $T < 500K$ , while the canonical orientation-averaged prescription does it at either  $T < 3500K$  for  $\gamma = 1$  or  $T < 2800K$  for  $\gamma = 0.25$ , and therefore, (*ii*) the parameterization of any of these orientation-average models for the modeling of the original anisotropic molecular fluid at very low density should embody the range of applicability of the perturbation expansions used in their derivation.

In Figure 2 we display the temperature dependence of the second virial coefficient for an actual polarizable Stockmayer (anisotropic) fluid in comparison with the corresponding free energy orientation-averaged and canonical orientation-averaged potential counterparts, as well as the adjusted canonical orientation-averaged potential proposed by Paul and Warnatz. {Paul, 1998 #15512} As expected, the second virial coefficient resulting from the free energy orientation-averaged potential exhibits the closest agreement with that of the actual anisotropic polarizable Stockmayer model fluid. For further enlightening in Figure 3 we compare the resulting second virial coefficient of the anisotropic polarizable Stockmayer fluid against that of either the first or both the first and second non-vanishing terms of the perturbation expansion of the Boltzmann factor. Not surprisingly, the incorporation of the second non-vanishing term increases the temperature at which the free energy orientation-averaged description is within the indicated accuracy.

### 3. PARAMETERIZATION OF THE EFFECTIVE LENNARD-JONES POTENTIAL

Transport properties and microstructure of fluids at normal conditions are typically more sensitive to short range repulsive interactions associated with the close-encounter particle collisions than, *e.g.*, the second virial coefficient that depends more directly on repulsive and attractive interactions. The immediate consequence of this feature is the proliferation of force-fields for popular model potentials whose thermodynamics-based parameterization results in unreliable descriptions of transport properties, while transport-based parameterizations generate poor thermodynamic representations. The pressing need here is to apply the acquired

Ariel Chialvo 5/25/2017 10:07 AM  
Comment [3]:

Ariel Chialvo 5/25/2017 10:13 AM  
Comment [4]:

understanding from the previous sections in the accurate force field parameterization of a model fluid able to describe simultaneously the thermodynamic and transport properties of rarified steam at extreme conditions.

#### *a Zero-density shear viscosity as input for the force-field parameterization*

By taking advantage of the availability of highly accurate data for the shear viscosity of water {Huber, 2009 #15528} and steam, {Teske, 2005 #15527; Hellmann, 2015 #15522} here we make contact between the data for the zero-density shear viscosity  $\eta_o$  and the underlying intermolecular interactions through the second-order solution of the kinetic theory of gases, *i.e.*, {Maitland, 1981 #370}

$$\eta_o(T) = 5(\pi m k T)^{0.5} f_\eta^{(2)} / 16\pi\sigma^2 \Omega^{(2,2)*} \quad (32)$$

where  $\Omega^{(2,2)*}$  is the reduced collision integral,  $\Omega^{(l,s)}/\pi\sigma^2$ ,  $m$  is the molecular mass,  $\sigma$  is the diameter from the normalization by the hard-sphere collision integral, and  $f_\eta^{(2)}$  is the correction factor associated with the second order solution given by, *i.e.*, {Kihara, 1953 #15529}

$$f_\eta^{(2)} = 1 + (3/49) \left( 4\Omega^{(2,3)*}/\Omega^{(2,2)*} - 7/2 \right)^2 \quad (33)$$

as a simpler alternative to the original Chapman and Cowling's factor, *i.e.*, {Chapman, 1939 #396}

$$f_\eta^{(2)} = 1 + \frac{3(7\Omega^{(2,2)*} - 8\Omega^{(2,3)*})^2}{(154\Omega^{(2,2)*}\Omega^{(2,2)*} + 80\Omega^{(2,4)*}\Omega^{(2,2)*} - 192\Omega^{(2,3)*}\Omega^{(2,3)*})} \quad (34)$$

The magnitude of  $f_\eta^{(2)}$  for a Lennard-Jones fluid deviates from unit by  $100(f_\eta^{(2)} - 1)/f_\eta^{(2)} < 0.72\%$  in the  $0.3 \leq T^* \equiv kT/\epsilon \leq 400$  range according to the most accurate collision integrals available to date {Kim, 2014 #15523}, *i.e.*,

$$\Omega^{(l,s)*}(T^*) = a^{(l,s)} + \sum_{i=1}^6 \left[ b_i^{(l,s)} (T^*)^{-i} + c_i^{(l,s)} (\ln T^*)^i \right] \quad S3-10$$

whose corresponding coefficients for  $(l,s)$  equal to (1,1), (1,2), (2,2) and (2,3) are displayed in Table D1. We should note that the collision integrals  $\Omega^{(l,s)*}(T^*)$  and  $\Omega^{(l,s+1)*}(T^*)$  are related by the following conditions (see Appendix S3 in the supplementary information document for details),

$$\Omega^{(l,s+1)*}(T^*) = \Omega^{(l,s)*}(T^*) + T^* \left( d\Omega^{(l,s)*}/dT^* \right) / (s+2) \quad (35)$$

$$\Omega^{(l,s+2)*}(T^*) = 2\Omega^{(l,s+1)*}(T^*) - \Omega^{(l,s)*}(T^*) + T^{*2} \left( d^2\Omega^{(l,s)*}/dT^{*2} \right) / [(s+1)(s+2)] \quad (36)$$

$$\Omega^{(l,s+3)*}(T^*) = 3\Omega^{(l,s+2)*}(T^*) - 3\Omega^{(l,s+1)*}(T^*) + \Omega^{(l,s)*}(T^*) + T^{*3} \left( d^3\Omega^{(l,s)*}/dT^{*3} \right) / [(s+1)(s+2)(s+4)] \quad (37)$$

and analogous  $\Omega^{(l,s+n)*}(T^*)$  expressions for  $n > 2$  that provide a simple check of consistency for the regressed coefficients in Eqn. S3-6 as illustrated in Appendix S3 (supplementary information document).

The force-field parameterization is consequently accomplished via fitting of the energy  $\varepsilon_{LJ}$  and size  $\sigma_{LJ}$  parameters in Eqn. (26) to the temperature dependence of the experimentally determined reduced collision integral  $\Omega^{(2,2)*}$ , *e.g.*, Eqn. (32), assuming  $f_\eta^{(2)} = 1$ . For this force-field optimization we have chosen the molecular polarizability  $\alpha = 1.444 \text{ \AA}^3$  {Eisenberg, 1969 #1391} and permanent dipole moment  $\mu = 1.855 D$  {Dyke, 1973 #6373} for the gas phase parameters of water, resulting in  $\varepsilon_{LJ} = 293.7 k(K)$  and  $\sigma_{LJ} = 2.920 \text{ \AA}$ , with

$\mathcal{S}(T) = 1 + 0.0988883 + 284.600188/T(K)$ . In Figure 4a we illustrate the behavior of the collision integral  $\Omega^{(2,2)}$  as determined from the most accurate data available for the temperature dependence of the zero-density shear viscosity of water {Hellmann, 2015 #15522}, after assuming  $f_\eta^{(2)} = 1$ , in comparison with the resulting orientation-averaged parameterization.

Ariel Chialvo 5/25/2017 1:11 PM  
Comment [5]:

### b Second virial coefficient of water as input for the force-field parameterization

The second virial coefficient describes the zero-density behavior of the fluid's residual volume, *i.e.*,  $\lim_{\rho \rightarrow 0} V^{res}(T, P) = (V - kT/P)/N = B(T)$ , a quantity available for water over a very

wide temperature range relevant to the processes commented in the introduction. For the purpose of force-field parameterization we invoke to the tabulated reduced virial  $B_v^*(T^*)$  {Maitland, 1981 #370; Hryniecki, 2011 #15067} regressed according the following expression,

$$B^*(T^*) = [1.9863T^{*(-0.25)} - 1.5985T^{*(-0.5)} - 6.7636T^{*(-1.5)} + 8.0952T^{*(-2.0)} - 4.8797T^{*(-2.5)} + 0.89417T^{*(-3.5)} - 0.25573T^{*(-4.0)} - 0.015386T^{*(-5.0)}] \quad (38)$$

where  $B^*(T^*) = B(T)/b_o$ ,  $b_o = 2\pi N_A \sigma_{eff}^3 / 3$ , within the  $0.3 \leq T^* \equiv kT/\varepsilon_{eff} \leq 10000$  range according to effective force-field parameters, Eqn. (27). In Figure 4b we display the temperature dependence of the second virial coefficient of water as described by the orientation-averaged effective potential in comparison with the accurate standard tabulation {Harvey, 2004 #3780} for  $298 \leq T(K) \leq 3000$ .

#### 4. RESULTING THERMODYNAMIC AND TRANSPORT PROPERTIES OF STEAM

In this section we illustrate the accuracy of the orientation-averaged effective potential, fitted to the second virial coefficient and zero-density shear viscosity in the preceding section, to represent other relevant thermodynamic and transport properties of water vapor. A stringent test of the accuracy of the resulting interaction potential is the adequate representation of the residual properties of the fluid,  $\mathcal{P}^{res}(T,P) = \mathcal{P}(T,P) - \mathcal{P}^{IG}(T,P)$ , *i.e.*, the isobaric-isothermal difference between the properties of the actual fluid and their zero-interaction counterparts, as a measure of the contribution of the intermolecular interactions to the fluid properties. {Chialvo, 1993 #1311}

For example, we can evaluate the residual Gibbs free energy of a rarified fluid, whose behavior obeys the first-order truncated virial EoS (see Appendix S4 in the supplementary information document), *i.e.*,

$$G^{res}(NPT) = -kT \ln(1 - N\beta PB) \equiv NPB \quad S4-14$$

and consequently,

$$H^{res}(NTP) = NP(B - TB_T) \quad S4-15$$

$$S^{res}(NTP) = -NPB_T \quad S4-16$$

$$C_p^{res}(NPT) = -NPTB_{TT}$$

S4-17

where  $B_T \equiv dB/dT$  and  $B_{TT} = dB_T/dT$ . Note also that the speed of sound  $\omega = (\partial P/\partial \rho)_S^{0.5}$  can be written as  $(\partial P/\partial \rho)_S^{0.5} = \sqrt{\gamma(\partial P/\partial \rho)_T}$ , consequently, in terms of the above thermal and volumetric properties of the low-density fluid as follows,

$$\omega_o^2 = \frac{(C_p^{IG} - NPTB_{TT})(1+2\rho B)^2 kT}{[C_p^{IG} - Nk - NP(B_T + TB_{TT})](1+2\rho B) - Nk(1+\rho B)^2} \quad (39)$$

$$\omega_o^2 = \frac{(C_p^{IG} - NPTB_{TT})[(1+3\beta BP)^2/(1+\beta BP)]kT}{[C_p^{IG} - Nk - NP(B_T + TB_{TT})](1+3\beta BP) - kT(1+2\beta BP)}$$

with  $C_p = C_p^{IG} - NPTB_{TT}$ ,  $C_v = C_p^{IG} - Nk - NP(B_T + TB_{TT})$ , and  $(\partial P/\partial \rho)_T = kT(1+2\rho B)$ , where we have expressed  $\rho B$  in terms of the variables  $P$  and  $T$ . In other words, the accurate representation of  $B(T)$  by the orientation-averaged potential of Section 3 provides, in principle, access to additional isobaric thermochemical properties and related quantities of the fluid under rarified conditions.

In Figures 5-10, where we use the *ab initio*  $B(T)$  correlation as the proxy for our model since it is the target of the parameter optimization, we display the isobaric-temperature and isothermal-pressure dependences of rarified steam residual Gibbs free energy, enthalpy and isobaric heat capacity as described by the orientation-averaged potential model in comparison with the actual behavior according to the IAPWS95-EoS. {Wagner, 2002 #3280} The agreement between the two sets of data in the isobaric comparison of Figures 5-7 highlights the accuracy of the representation of  $B(T)$  and its  $T$ -derivatives. Note that the IAPWS95-EoS predictions span up to  $T = 1273K$ , i.e., its upper temperature bound, while the orientation-averaged model involves no temperature upper limit. The isothermal comparison between the model predictions and IAPWS95-EoS correlations, within the pressure range where the truncated second virial-EoS is an accurate representation, emphasizes the role played by the pressure and temperature pre-factors in magnifying the inaccuracies of the  $B(T)$  representation by the model. Since  $B(T)$  has been used as the thermodynamic (together with the zero density shear viscosity as the

Ariel Chialvo 5/25/2017 1:12 PM

**Comment [6]:**

transport) property for the adjustment of the orientation-averaged model, the observed disagreement in Figures 8-10 is simply a manifestation of the discrepancies between the IAPWS95-EoS correlated and the *ab initio* based tabulation for  $B(T)$ . In fact, in Figure 11 we compare the two representations in the high temperature range where becomes evident the increasing deviation between the two correlations that reaches about 10% at the maximum temperature handled by the IAPWS95-EoS. Thus, it becomes rather clear that the required accurate description of the thermodynamic (residual) properties of the rarified fluid – the ones accounting for the intermolecular interactions – hinges around the proper representation of the temperature dependence of the second virial coefficient as highlighted by Eqns. E14-E17 and 39.

Ariel Chialvo 5/25/2017 9:57 AM  
Comment [7]:

Even though other transport properties of water have been measured and tabulated over wide ranges of state conditions, including shear viscosity {Huber, 2009 #15528} and thermal conductivity, {Huber, 2012 #15520} there is an evident lack of experimental data for the self-diffusion coefficient of steam. In fact, as far as we are aware there are only a handful of sources of experimental data from Swinton's mass spectrometry {Swinton, 1971 #15513} for  $363 \leq T(K) \leq 517$  and NMR spin-echo techniques including that of Lamb *et al.* {Lamb, 1981 #1643} for  $673 \leq T(K) \leq 973$  and  $\rho(g/cc) \geq 0.1$ , and Yoshida *et al.* {Yoshida, 2005 #3684; Yoshida, 2007 #3924} for  $473 \leq T(K) \leq 673$  and  $0.0041 \leq \rho(g/cc) \leq 0.0056$ . This scenario highlights the urgency behind alternative means for the estimation of the self-diffusivity of steam at extreme conditions.

From a theoretical standpoint the low-density self-diffusion coefficient of steam,  $D_o$ , can be computed through the solution of the Boltzmann equation, *i.e.*, {Maitland, 1981 #370}

$$D_o(T, P) = 3(\pi m k T)^{0.5} f_{\mathcal{D}}^{(2)} / 8 \rho \pi \sigma^2 \Omega^{(1,1)*} \quad (40)$$

where  $f_{\mathcal{D}}^{(2)}$  is the correction factor associated with the second order solution, *i.e.*,

$$f_{\mathcal{D}}^{(2)} = 1 + \frac{(6\Omega^{(1,2)*} - 5\Omega^{(1,1)*})^2}{\Omega^{(1,1)*} [30(\Omega^{(1,1)*} - \Omega^{(1,2)*}) + 16(\Omega^{(2,2)*} - \Omega^{(1,3)*})] - 36(\Omega^{(1,2)*})^2} \quad (41)$$

According to the collision integrals from Kim & Monroe, {Kim, 2014 #15523} the magnitude of  $f_{\mathcal{D}}^{(2)}$  for a Lennard-Jones fluid deviates from unity by  $100(f_{\mathcal{D}}^{(2)} - 1)/f_{\mathcal{D}}^{(2)} < 0.78\%$  in the

$0.3 \leq T^* \leq 400$  range, therefore, we can safely assume  $f_D^{(2)} = 1$  in our calculations. Moreover, the fluid density  $\rho$  in the denominator of Eqn. (40) can be accurately described at the second virial coefficient level, *i.e.*,

$$\rho(T, P) = (2B)^{-1} \left[ -1 + \left( 1 + 4B\beta P / N_A \right)^{0.5} \right] \quad (42)$$

resulting from the meaningful root of the truncated virial equation  $P = kT\rho(1 + B\rho)$ , where  $N_A$  is Avogadro's number.

## 5. CONCLUDING REMARKS

We have addressed the fundamentals underlying the development of an orientation-averaged intermolecular potential model for the accurate computation of relevant thermodynamics and transport properties of rarified steam over a wide range of temperature typically encountered in highly energetic environments including aircraft turbines, rocket engines and metal-steam power generators. We have discussed the reliability of the approach and the accuracy of the resulting models by addressing **the three proposed questions** in the introduction, in addition to the careful/rigorous (simultaneous) force-field parameterization against the temperature dependence of the second virial coefficient and the zero-density shear viscosity of steam, through the direct comparison between the model predictions of the temperature dependence of the (residual) Gibbs free energy, enthalpy, isobaric and isochoric heat capacities, speed of sound, **(zero-density thermal conductivity?)**, and low-density self-diffusion.

The significance underlying the above model predictions becomes more evident by considering the effect of real gas nonideality on the chemical equilibria involving extreme reactive gaseous environments such as those encountered in the combustion of hydrogen in the *RS-25* rocket engine, {Rocketdyne, 1998 #15514} where this effect would (and could) be accurately described at the first-order truncated virial perturbation. In fact, let us consider the main oxidation reaction, *i.e.*,



for which the fugacity-based thermodynamic equilibrium constant becomes,

Ariel Chialvo 5/25/2017 2:19 PM  
Comment [8]:

$$K_f(T) = \left[ \hat{\phi}_{H_2O} x_{H_2O} / \hat{\phi}_{H_2} x_{H_2} \right]^2 / \left[ P \hat{\phi}_{O_2} x_{O_2} \right] \quad (44)$$

$$= \underbrace{K_p(T)}_{IG} \underbrace{K_\phi(T)}_{NI}$$

where  $\hat{\phi}_i = \exp(\hat{g}_i^{res}/RT)$  is the partial fugacity coefficient of the  $i$ -species associated to the partial molar Gibbs free energy  $\hat{g}_i^{res}$ , while  $IG$  and  $NI$  highlight the contributions of the ideal gas and the non-ideal (residual) contributions to the thermodynamic equilibrium constant, respectively. Alternatively, we could express the effect of gas nonideality on the conventional isothermal-isobaric displacement  $\xi$  of the chemical reaction as follows,

$$(dG^{res}(\xi)/d\xi)_{TP} = RT \left( 2 \ln \hat{\phi}_{H_2O} - 2 \ln \hat{\phi}_{H_2} - \ln \hat{\phi}_{O_2} \right) \quad (45)$$

with  $\xi \equiv (N_i - N_i^o)/v_i$ , while  $N_i^o$  and  $v_i$  denote the initial number of molecules for the  $i$ -species and corresponding stoichiometric coefficient. The partial fugacity coefficient of the  $i$ -species in Eqn. (45) can be expressed in terms of the corresponding pure  $i$ -component residual Gibbs free energy, and a quadratic combination of the second virial coefficients for all  $ab$ -pair interactions in the mixture as follows,

$$\hat{\phi}_i(PTx) = \exp\left(G_{purei}^{res}/NRT\right) \exp\left\{(P/2RT) \sum_{kl} x_k x_l (2\delta_{ki} - \delta_{kl})\right\} \quad (46)$$

with  $\delta_{ab}(T) = 2B_{ab} - B_{aa} - B_{bb}$  (*e.g.*, see Appendix E of Ref. {Chialvo, 2008 #4721}). Note however that when  $\lim_{T \rightarrow \text{very high}} \delta_{ab}(T) \sim 0$ , the molecular asymmetries embodied in  $\delta_{ab}(T)$  become negligibly small, and consequently, the gaseous system would behave as an ideal solution in the Lewis-Randall sense {O'Connell, 2005 #14710}, *i.e.*,  $B_{ab} = 0.5(B_{aa} + B_{bb})$  so that Eqn. (46) would reduces,

$$\lim_{\delta_{ab} \rightarrow 0} \hat{\phi}_i(PTx) = \exp\left(G_{purei}^{res}/NRT\right) \quad (47)$$

Moreover, under those conditions we could also determine how the temperature and pressure rate of change of the gas nonideality would affect the equilibrium constant, Eqn. (44), and the reaction displacement, Eqn. (45), according to the corresponding derivatives of Eqn. (47), *i.e.*,

$$\begin{aligned} \lim_{\delta_{ab} \rightarrow 0} \left( \partial \ln \hat{\phi}_i / \partial T \right)_{Px} &= -H_{purei}^{res} / NRT^2 \\ &= -P(B - TB_r)_{purei} / RT^2 \end{aligned} \quad (48)$$

$$\begin{aligned} \lim_{\delta_{ab} \rightarrow 0} \left( \partial \ln \hat{\phi}_i / \partial P \right)_{Tx} &= V_{purei}^{res} / NRT^2 \\ &= B_{purei}(T) \end{aligned} \quad (49)$$

Thus, the orientation-averaged potential provides a versatile approach for the accurate calculation of the thermodynamic residual properties of the rarified fluids, whose results can be incorporated into routines for the self-consistent calculation of thermodynamic and transport properties of fluids in extreme environments as long as we identify the range of validity of the model parameterization.

In passing, we should note on the one hand that some popular programs for complex chemical equilibrium calculations, including NASA's CEA2 code {Gordon, 1994 #15962} and its numerous adaptations,{Bishnu, 2001 #15992}, as well as TEA {Blecic, 2016 #15998} and TECA {Venot, 2012 #15999} involve the thermodynamics of ideal gas mixtures, a behavior that cannot be guaranteed when dealing with either combustion in modern rocket engines (such as the *RS-25* {Rocketdyne, 1998 #15514} and the Raptor engines {<http://spaceflight101.com/spx/spacex-raptor/>, 2019 #15994}) whose chamber pressures are higher than 20MPa, or extreme exoplanet environments comprising pressures up to 100MPa. {Drummond, 2016 #15997;Stock, 2018 #15995} On the other hand, we must highlight some emerging issues regarding the concomitant modeling of the thermodynamic and transport properties of rarified polar fluids. For example, from Eqns. (13) and (15) we have that,

$$\begin{aligned} \Phi_{12}(r) = \langle \phi(r) \rangle_{\omega}^{canon} + (\beta/2) \langle \phi_{12}^2(r, \omega) \rangle_{\omega} - (\beta^2/3) \langle \phi_{12}^3(r, \omega) \rangle_{\omega} + \\ (\beta^3/8) \langle \phi_{12}^4(r, \omega) \rangle_{\omega} - \dots \end{aligned} \quad (49)$$

and consequently, we expect that,

$$\Phi_{12}(r) \xrightarrow[\text{as } T \text{ increases}]{\text{approaches}} \langle \phi(r) \rangle_{\omega}^{canon} \quad (50)$$

Moreover, it becomes clear that the orientation-averaged counterparts of the polarizable Stockmayer anisotropic potential described in Appendix A exhibit precisely such a behavior as depicted in Figures 1-2 where we display the comparison of their radial profile and the corresponding temperature dependence of the resulting virial coefficients, respectively. The two averaged potentials are in general distinct by definition, and consequently, care must be exercised when using them for modeling purposes. Obviously, a ‘parameter adjusting’ of either potential can result in identical (albeit artificial) representations (*e.g.*, same  $\sigma_{\text{eff}}(T)$  and  $\varepsilon_{\text{eff}}(T)$  but different  $\sigma_L$  and  $\varepsilon_L$ ) as clearly depicted by the choice of  $\gamma = 0.5$  in Paul and Warnatz’s representation, {Paul, 1998 #15512} *i.e.*,  $\Phi_{12}(r) = \langle \phi(r, \gamma = 0.5) \rangle_{\omega}^{\text{canon}}$ .

Ariel Chialvo 5/9/2017 2:46 PM  
Comment [9]:

In addition, we should note here some encountered discrepancies between the coefficients of the second terms of our Eqns. (19)-(20) and those in Eqns. (8)-(9) from Danon and Amdur work, {Danon, 1969 #15509} including their magnitude and sign, even when their Eqns. (8)-(9) satisfy the condition given by our Eqn. (10). In fact, Danon and Amdur reported  $(7\beta^3/450)$  and  $(14\beta^3/225)$  to be the coefficients of the second terms for the free energy and canonical based orientation-averaged potentials, while we derived them by symbolic integration via Mathematica (© 2017 Wolfram) in Appendix S1 (of the supplementary information document) resulting in  $(-\beta^3/25)$  and  $(-4\beta^3/25)$ , respectively. Their results have been quoted frequently in the early literature, {Singh, 1971 #15506; Malik, 1974 #15977; Singh, 1980 #15978; Pathak, 1981 #15979; Pathak, 1981 #15980} and we are not aware of any publication either contesting or correcting this issue.

As we argued in §4, experimental data for the self-diffusion coefficient of steam at very low density or rarified conditions are quite scarce, a situation that hinders the testing and validation of new correlation and formalisms. This shortage, however, offers the unmatched opportunity for molecular simulation to help with the missing data provided that we have available a proven reliable intermolecular potential model able to describe accurately the equilibrium and dynamics properties of water over wide ranges of state conditions.

Ariel Chialvo 5/14/2017 8:43 AM  
Comment [10]:

Here we can envision two alternative and practical routes for the computation of the self-diffusion coefficient of rarified steam. The first one takes advantage of the availability of accurate experimental data for the zero-density shear viscosity  $\eta_o(T^*)$  of steam, {Teske, 2005}

#15527;Hellmann, 2015 #15522} by invoking the kinetic theory relation between low-density self-diffusivity and zero-density shear viscosity, *i.e.*,

$$\mathcal{D}_o(T^*, P^*)/\eta_o(T^*) = 6f_{\mathcal{D}}^{(2)}\Omega^{(2,2)*}/5f_\eta^{(2)}\rho\Omega^{(1,1)*} \quad (51)$$

where  $f \equiv f_{\mathcal{D}}^{(2)}/f_\eta^{(2)}$  deviates by  $100(f-1)/f < 0.06\%$  from unity in the  $0.3 \leq T^* \leq 400$  range, and consequently we can just set  $f_{\mathcal{D}}^{(2)}/f_\eta^{(2)} = 1$  in Eqn. (51) for our calculations. Thus, according to the parameterized orientation-average potential to the zero-density shear viscosity we can define  $T^* = kT/\varepsilon_{eff}$ , and consequently, by introducing the accurate experimental data of  $\eta_o(T)$ , and after invoking Eqn. (42) for the density of rarified steam, we are able to generate reliable data for the corresponding self-diffusion coefficient  $\mathcal{D}_o(T^*, P^*)$  from Eqn. (51). In Figure 12 we display the self-diffusion coefficient  $\mathcal{D}_o(T, P = 1.0\text{bar})$  as predicted by Eqn. (51) when introducing the most accurate values of the zero-density shear viscosity  $\eta_o(T)$  from the available literature {Hellmann, 2015 #15522}, after invoking Eqn. (42) and the second virial coefficient given by the correlation of Harvey and Lemmon {Harvey, 2004 #3780}, in comparison with two data sources. While the three representations provide essentially the same outcome for  $T < 1700K$ , there is a small but clear negative deviation of the present shear-viscosity based prediction with respect to the earlier correlations.

Ariel Chialvo 5/5/2017 11:01 AM  
Comment [11]:

The second conceived route to accurate self-diffusion coefficients of rarified steam comprises its direct computation via molecular dynamics simulation involving a very accurate water intermolecular potential {Yoshida, 2006 #3683;Yoshida, 2007 #3924}. For illustration purposes, and as part of a separate broader study, we have run isothermal-isochoric molecular dynamics simulations of the GCP water model {Paricaud, 2005 #3413;Chialvo, 2015 #14233} to compute the self-diffusion coefficient of rarified steam over the  $473 \leq T(K) \leq 2500$  range at  $\rho = 0.001\text{g/cm}^3$ , and at  $0.0041 \leq \rho(\text{g/cm}^3) \leq 0.051$  within  $473 \leq T(K) \leq 673$  range to make direct contact with the most recent NMR-based experimental data of Yoshida *et al.* {Yoshida, 2006 #3683;Yoshida, 2007 #3924}. A brief description of the relevant details about the simulation methodology and related computation of the self-diffusion of rarified steam are given in Appendix D. The comparison in Figure 13 between simulation results for the GCP water

Ariel Chialvo 5/25/2017 1:54 PM  
Comment [12]:  
Ariel Chialvo 5/25/2017 2:19 PM  
Comment [13]:

model at  $\rho = 0.001 \text{ g/cm}^3$ , NMR measurements at  $\rho = 0.0041 \text{ g/cm}^3$  {Yoshida, 2006}

#3683; Yoshida, 2007 #3924}, and the kinetic theory prediction for the product of the system pressure and the low-density self-diffusion coefficient  $P\mathcal{D}_o$ ,

$$P\mathcal{D}_o = 6f_D^{(2)}\Omega^{(2,2)*}\eta_o(T^*)P/5f_\eta^{(2)}\rho\Omega^{(1,1)*} \quad (52)$$

for which  $\lim_{\rho \rightarrow 0} P\mathcal{D}_o = 6f_D^{(2)}\Omega^{(2,2)*}\eta_o(T^*)kT/5f_\eta^{(2)}\Omega^{(1,1)*}$ , *i.e.*, a quantity depending only on the

temperature  $T$ , lends support to the accuracy of both, the parameterized collision integrals to the zero-density shear viscosity and the GCP water model, in describing the self diffusion coefficient of rarified steam.

In summary, orientation-averaged intermolecular potential models become successful alternative approaches to the description of the thermophysical behavior of polar-polarizable fluids at rarified extreme conditions (such as ultrahigh temperature steam) through the simultaneous optimization of the energy and size parameters for the reference fluid fitted to a pair of experimentally accurate zero-density, *i.e.*, one thermodynamic and one transport, quantities such as the second virial coefficient and the zero-density shear viscosity.

#### ACKNOWLEDGEMENTS

As a belated acknowledgement, one of us would like to thank Carl A. Aukerman at NASA Lewis (now Glenn) Research Center, who in the early 1970's provided a copy of Sanford Gordon's report on the equilibrium of JP-4/LOX combustion gases, Ref. {Huff, 1956 #15985}, and ignited AAC's interest on the thermodynamic and transport behavior of rarified gases at extreme conditions.

## APPENDIX A: Polarizable Stockmayer potential model

Let us consider a pair of molecules each one characterized by a permanent point dipole  $\boldsymbol{\mu}_i$  with an embedded scalar point dipole polarizability  $\alpha_i$ , *i.e.*,

$$\mathbf{m}_1 = \alpha_1 \hat{T}_{12} \cdot (\boldsymbol{\mu}_2 + \mathbf{m}_2) \quad \text{A1}$$

$$\mathbf{m}_2 = \alpha_2 \hat{T}_{21} \cdot (\boldsymbol{\mu}_1 + \mathbf{m}_1) \quad \text{A2}$$

where  $\mathbf{m}_i$  is the yet unknown induced dipole moment at the location of the dipole polarizability  $\alpha_i$ , and  $\hat{T}_{ij} \cdot (\boldsymbol{\mu}_j + \mathbf{m}_j) = \hat{T}_{ij} \cdot \mathbf{d}_j$  is the corresponding dipole electric field, with

$$\hat{T}_{ij} = r_{ij}^{-3} [3\hat{r}_{ij}\hat{r}_{ij} - I] \quad \text{A3}$$

where  $\hat{r}_{ij} \equiv \mathbf{r}_{ij}/|\mathbf{r}_{ij}|$  and  $I$  denote unit vector and matrix, respectively. To assess the magnitude and direction of the induced dipole moments  $\mathbf{m}_1$  and  $\mathbf{m}_2$  we must solve the A1-A2 system of equations, *i.e.*,

$$\mathbf{m}_1 = [\alpha_1 \hat{T}_{12} \cdot (\boldsymbol{\mu}_2 + \alpha_1 \hat{T}_{12} \cdot \boldsymbol{\mu}_1)] [I - \alpha_1 \alpha_2 \hat{T}_{12} \cdot \hat{T}_{21}]^{-1} \quad \text{A4}$$

$$\mathbf{m}_2 = [\alpha_2 \hat{T}_{21} \cdot (\boldsymbol{\mu}_1 + \alpha_2 \hat{T}_{21} \cdot \boldsymbol{\mu}_2)] [I - \alpha_1 \alpha_2 \hat{T}_{12} \cdot \hat{T}_{21}]^{-1} \quad \text{A5}$$

where the second factor in A4-A5 represent the inverse of the bracket matrix. For example, if for the sake of illustration we choose the  $x$ -axis of the Cartesian coordinates of our system to be parallel to the vector joining the two polar particles,  $\mathbf{r}_{12}$  in Figure A1, then we have that,

Ariel Chialvo 4/28/2017 3:02 PM  
Comment [14]:

$$\begin{bmatrix} m_{xi} \\ m_{yi} \\ m_{zi} \end{bmatrix} = r_{ij}^{-3} \left\{ \begin{bmatrix} 2\alpha_i & 0 & 0 \\ 0 & -\alpha_i & 0 \\ 0 & 0 & -\alpha_i \end{bmatrix} \begin{bmatrix} \mu_{xj} \\ \mu_{yj} \\ \mu_{zj} \end{bmatrix} + \right. \\
\left. r_{ij}^{-3} \begin{bmatrix} 4\alpha_i\alpha_j & 0 & 0 \\ 0 & \alpha_i\alpha_j & 0 \\ 0 & 0 & \alpha_i\alpha_j \end{bmatrix} \begin{bmatrix} \mu_{xi} \\ \mu_{yi} \\ \mu_{zi} \end{bmatrix} \right\} \times$$

$$\begin{bmatrix} (1-4\alpha_i\alpha_j/r_{ij}^6)^{-1} & 0 & 0 \\ 0 & (1-\alpha_i\alpha_j/r_{ij}^6)^{-1} & 0 \\ 0 & 0 & (1-\alpha_i\alpha_j/r_{ij}^6)^{-1} \end{bmatrix} \quad \text{A6}$$

and consequently,

$$\begin{aligned}
d_{xi} &= (\mu_{xi} + 2\alpha_i\mu_{xj}r_{ij}^{-3})[1-4\alpha_i\alpha_j/r_{ij}^6]^{-1} \\
d_{yi} &= (\mu_{yi} - \alpha_i\mu_{yj}r_{ij}^{-3})[1-\alpha_i\alpha_j/r_{ij}^6]^{-1} \\
d_{zi} &= (\mu_{zi} - \alpha_i\mu_{zj}r_{ij}^{-3})[1-\alpha_i\alpha_j/r_{ij}^6]^{-1}
\end{aligned} \quad \text{A7}$$

for  $i \neq j = 1, 2$ .

Now, starting from the expression for the dipolar energy of this system {Vesely, 1977 #12333}, i.e.,

$$\phi_{12}^{ud}(\mathbf{r}, \boldsymbol{\omega}) = -0.5(\boldsymbol{\mu}_1 \cdot \hat{T}_{12} \cdot \mathbf{d}_2 + \boldsymbol{\mu}_2 \cdot \hat{T}_{21} \cdot \mathbf{d}_1) \quad \text{A8}$$

and after invoking the  $\alpha$ -expansion of the denominators in A7,  $[1-ax]^{-1} \approx 1+ax$ , A8 becomes approximated as follows,

$$\begin{aligned}
\phi_{12}^{ud}(\mathbf{r}, \boldsymbol{\omega}) &\equiv (\mu_1\mu_2/r_{12}^3)(\sin\theta_1\sin\theta_2\cos\varphi_{12} - 2\cos\theta_1\cos\theta_2) - \\
&\quad (0.5/r_{12}^6)[\alpha_1\mu_2^2(3\cos^2\theta_2+1) + \alpha_2\mu_1^2(3\cos^2\theta_1+1)] + \dots \\
&= \phi_{12}^{\mu\mu}(\mathbf{r}, \boldsymbol{\omega}) + \phi_{12}^{\mu\alpha}(\mathbf{r}, \boldsymbol{\omega})
\end{aligned} \quad \text{A9}$$

which is Eqn. (22) in the main text. To make such a link clearer we invoke Figure A1, from which we can highlight the following identities:

$$(\hat{\boldsymbol{\mu}}_i \cdot \hat{r}_{ij}) = \cos \theta_i \quad \text{A10}$$

where  $\hat{\boldsymbol{\mu}}_i = \boldsymbol{\mu}_i / |\boldsymbol{\mu}_i|$  describes the dipolar unit vector;

$$\hat{\boldsymbol{\mu}}_i \cdot \hat{\boldsymbol{\mu}}_j = \cos \gamma_{ij} = \cos \theta_i \cos \theta_j + \sin \theta_i \sin \theta_j \cos \varphi_{ij} \quad \text{A11}$$

with

$$\hat{\boldsymbol{\mu}}_i \cdot \hat{T}_{ij} \cdot \hat{\boldsymbol{\mu}}_j = r_{ij}^{-3} [ 3(\hat{\boldsymbol{\mu}}_i \cdot \hat{r}_{ij})(\hat{r}_{ij} \cdot \hat{\boldsymbol{\mu}}_j) - \hat{\boldsymbol{\mu}}_i \cdot \hat{\boldsymbol{\mu}}_j ] \quad \text{A12}$$

and finally,

$$\begin{aligned} \boldsymbol{\mu}_i \cdot \hat{T}_{ij} \cdot \hat{T}_{ji} \cdot \boldsymbol{\mu}_i &= r_{ij}^{-6} [ 3(\hat{\boldsymbol{\mu}}_i \cdot \hat{r}_{ij})\hat{r}_{ij} - \hat{\boldsymbol{\mu}}_i ] \cdot [ 3\hat{r}_{ji}(\hat{r}_{ji} \cdot \hat{\boldsymbol{\mu}}_i) - \hat{\boldsymbol{\mu}}_i ] \\ &= r_{ij}^{-6} [ 9(\hat{\boldsymbol{\mu}}_i \cdot \hat{r}_{ij})(\hat{\boldsymbol{\mu}}_i \cdot \hat{r}_{ji})(\hat{r}_{ij} \cdot \hat{r}_{ji}) - 6(\hat{\boldsymbol{\mu}}_i \cdot \hat{r}_{ij})^2 + (\hat{\boldsymbol{\mu}}_i \cdot \hat{\boldsymbol{\mu}}_i) ] \\ &= r_{ij}^{-6} [ 3\cos \theta_i + 1 ] \end{aligned} \quad \text{A13}$$

for  $i \neq j = 1, 2$ .

As a matter of illustration of the accuracy underlying the perturbation expansion embodied in A9, in Figure A2 we display a comparison between the outcome for the radial behavior of A9 and that from the corresponding exact solution of A8 for random molecular orientations of the pair of dipoles. As clearly evidenced in Figure A2, even for a significant size of dipole polarizability, A9 is a rather accurate representation for the dipole polarization energy.

## FIGURE CAPTIONS

Figure 1: Temperature evolution of the logarithm of the orientation-averaged Boltzmann factor for the anisotropic polarizable Stockmayer potential,  $-\ln\left\langle e^{-\beta\phi_{12}(\tau_{12},\omega_1,\omega_2)}\right\rangle_\omega$ , in comparison with three resulting first-order orientation-averaged potentials, , corresponding to the so-called free energy orientation-averaged ( $f=1$ ) and canonical orientation-averaged ( $f=2$ ) potentials, as well as the adjusted canonical orientation-averaged ( $f=0.5$ ) potential proposed by Paul and Warnatz {Paul, 1998 #15512} with  $\mu=1.855D$ ,  $\alpha=1.444\text{\AA}^3$ ,  $\sigma=2.92\text{\AA}$  and  $\varepsilon/k=283.7(K)$ .

Figure 2: Temperature dependence of the second virial coefficient for an actual polarizable Stockmayer (anisotropic) fluid in comparison with the corresponding free energy orientation-averaged and canonical orientation-averaged potential counterparts, as well as the adjusted canonical orientation-averaged potential proposed by Paul and Warnatz {Paul, 1998 #15512}.

Figure 3: Temperature dependence of the second virial coefficient for an actual polarizable Stockmayer (anisotropic) fluid in comparison with the first, Eqn. (27), and second non-vanishing perturbation expansion terms, Eqn. (30), of the free energy orientation-averaged potentials.

Figure 4: (a) Collision integral  $\Omega^{(2,2)}$  and (b) second virial coefficient  $B(T)$  for the orientation-averaged effective steam potential fitted to the most accurate available zero-density shear viscosity experimental data {Hellmann, 2015 #15522} and ab initio based correlation of the second virial coefficient of water {Harvey, 2004 #3780}, respectively.

Figure 5: Temperature dependence of the residual Gibbs free energy of rarified steam at  $P=1.0\text{ bar}$  according to the IAPWS95-EoS {Wagner, 2002 #3280} in comparison with the predicted behavior by the orientation-averaged potential model.

Figure 6: Temperature dependence of the residual enthalpy of rarified steam at  $P=1.0\text{ bar}$  according to the IAPWS95-EoS {Wagner, 2002 #3280} in comparison with the predicted behavior by the orientation-averaged potential model.

Figure 7: Temperature dependence of the residual isobaric heat capacity of rarified steam at  $P=1.0\text{ bar}$  according to the IAPWS95-EoS {Wagner, 2002 #3280} in comparison with the predicted behavior by the orientation-averaged potential model.

Figure 8: Pressure dependence of the residual Gibbs free energy of rarified steam at  $T=1250K$  according to the IAPWS95-EoS {Wagner, 2002 #3280} in comparison with the predicted behavior by the orientation-averaged potential model.

Figure 9: Temperature dependence of the residual enthalpy of rarified steam at  $T = 1250K$  according to the IAPWS95-EoS {Wagner, 2002 #3280} in comparison with the predicted behavior by the orientation-averaged potential model.

Figure 10: Temperature dependence of the residual isobaric heat capacity of rarified steam at  $T = 1250K$  according to the IAPWS95-EoS {Wagner, 2002 #3280} in comparison with the predicted behavior by the orientation-averaged potential model.

Figure 11: Temperature dependence of the second virial coefficient according to IAPWS95-EoS {Wagner, 2002 #3280} and the corresponding percentage deviation of the accurate *ab initio*-based correlation {Harvey, 2004 #3780} from the IAPWS95-EoS representation.

Figure 12: Kinetic theory shear-viscosity based prediction of the temperature dependence of the low-density self-diffusion coefficient of steam at  $P = 1.0bar$  in comparison with the two available datasets.

Figure 13: Comparison between the GCP water model at  $\rho = 0.001g/cm^3$  and the kinetic theory predictions for the product of the system pressure and the low-density self-diffusion coefficient  $PD_o$ .

Figure A1: Orientations defining the point dipole plus polarizability interaction potential

Figure A2: Comparison between the approximation A9 and that from the corresponding exact, *i.e.*, self consistent field, solution of A8 for randomly generated molecular orientations,  $\gamma_{12} = \arccos(\hat{\mu}_1 \cdot \hat{\mu}_2)$ , of a pair of polarizable point dipoles with  $\mu = 1.855D$  and  $\alpha = 1.444\text{\AA}^3$ .

Figure A3: Comparison of the behavior of the orientation-averaged potential

$\Phi_{12}(r) = -kT \ln \left\langle e^{-\beta\phi_{12}(\gamma_{12}, \omega_1, \omega_2)} \right\rangle_\omega$  for (a) the self-consistent polarizable Stockmayer model and (b) the first-order  $\alpha$ -perturbation expansion model for a pair of polarizable point dipoles described by  $\mu = 1.855D$  and  $\alpha = 1.444\text{\AA}^3$ , with the Lennard-Jones parameters  $\sigma = 2.92\text{\AA}$  and at  $T = 300K$ .

Figure D2: Log-log representation of the time dependence of the mean-squared displacement of rarified steam at  $\rho = 0.001g/cm^3$  and  $T = 1000K$  as described by the GCPM water intermolecular potential. The straight lines highlight the slopes of the short- and long-time asymptotic behavior resulting from the ballistic (slope=2) and diffusive (slope=1) dynamic regimes, respectively.

CITED REFERENCES

Figure 1

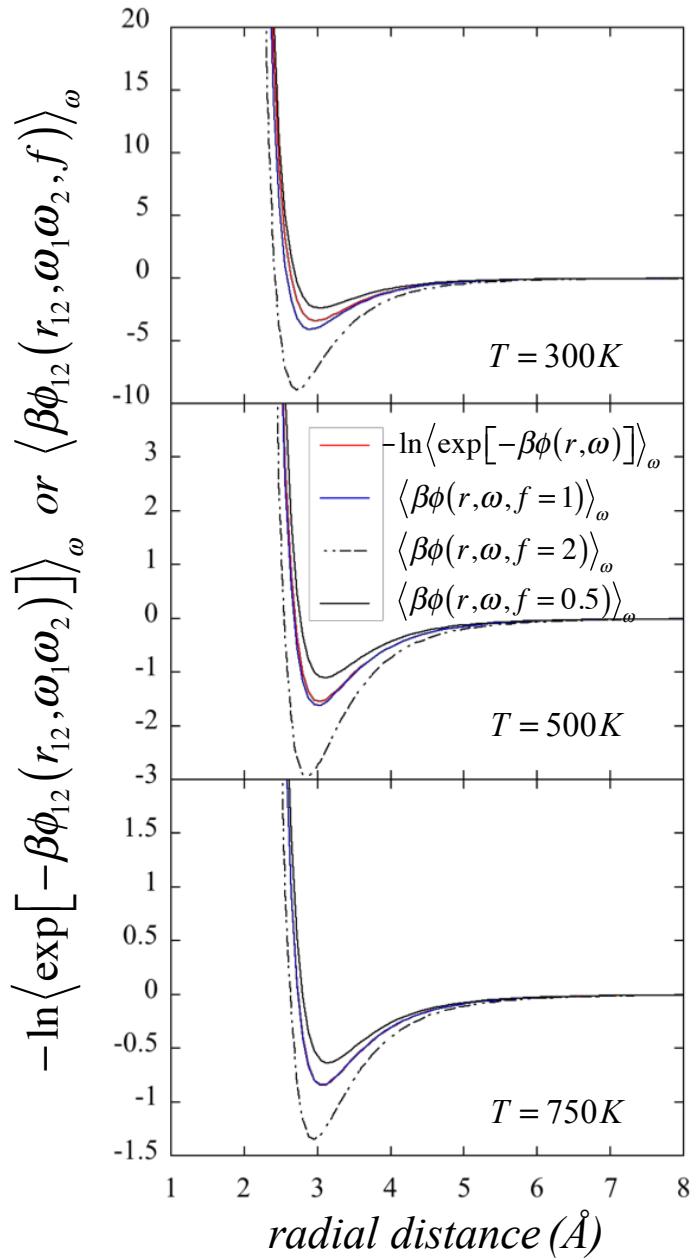


Figure 2

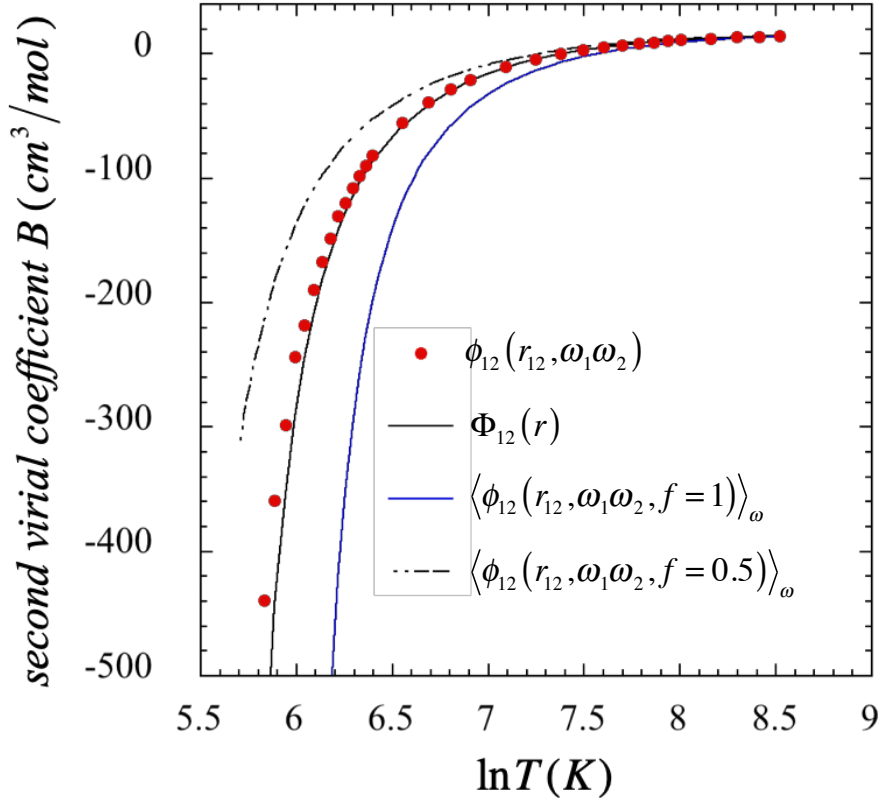


Figure 3

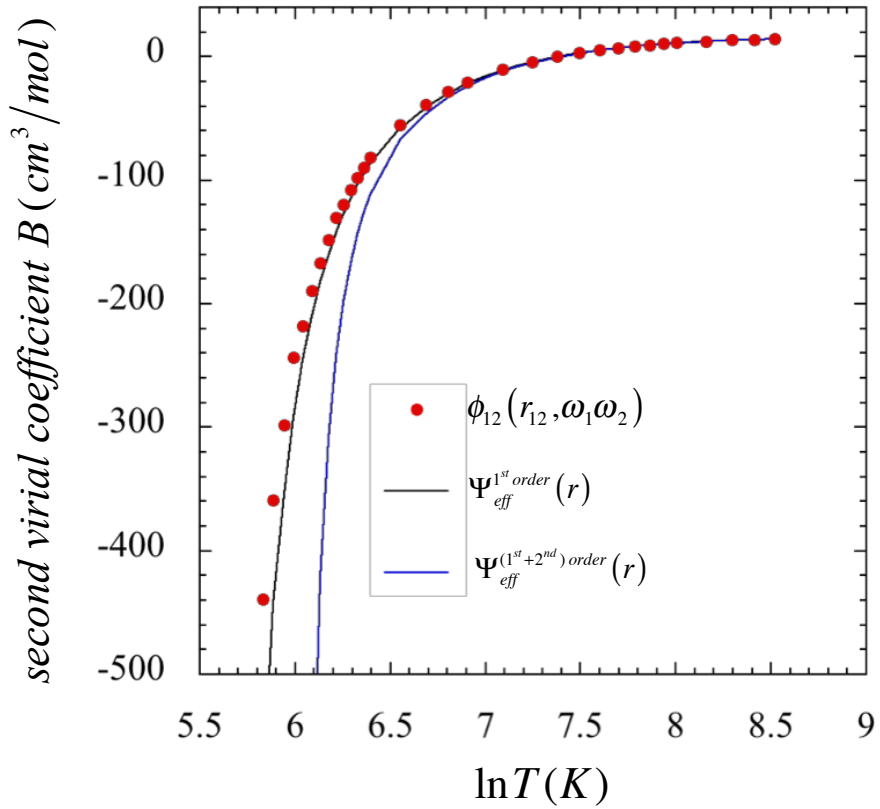


Figure 4

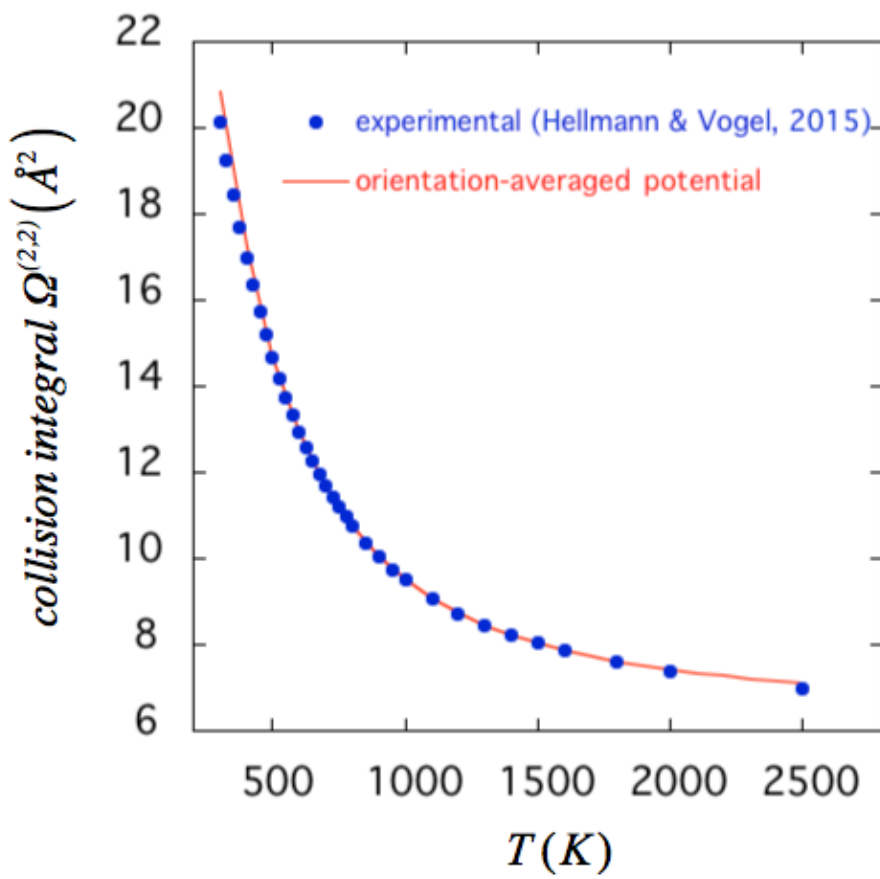


Figure 5

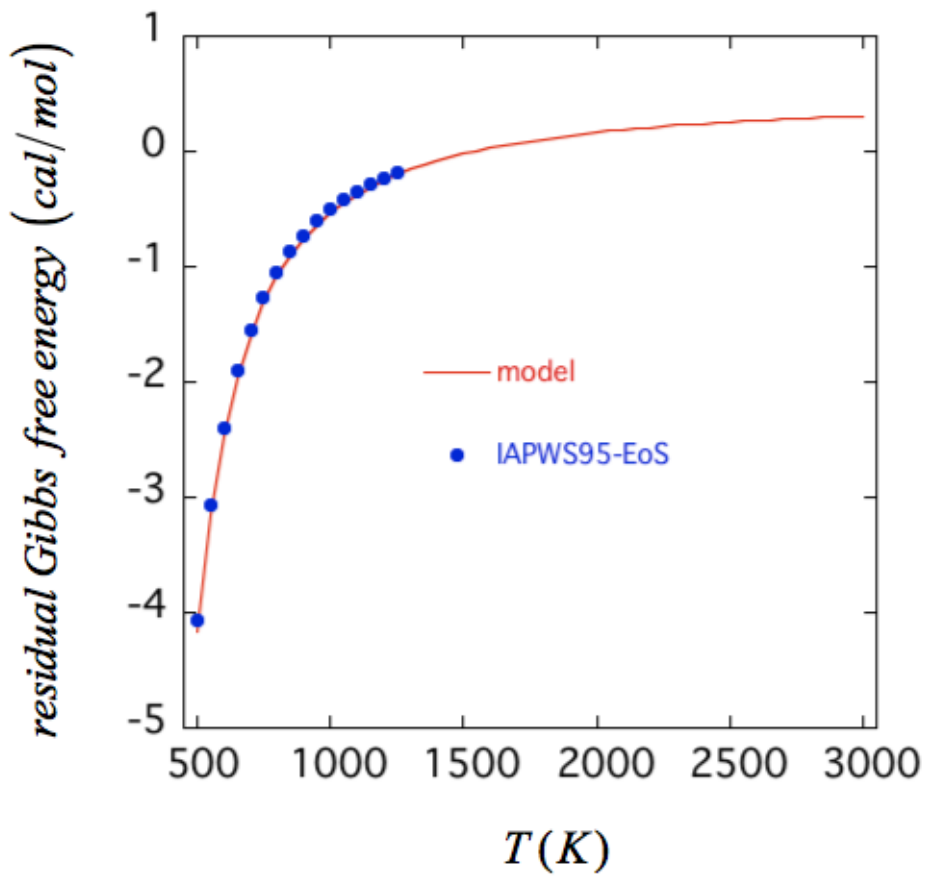


Figure 6

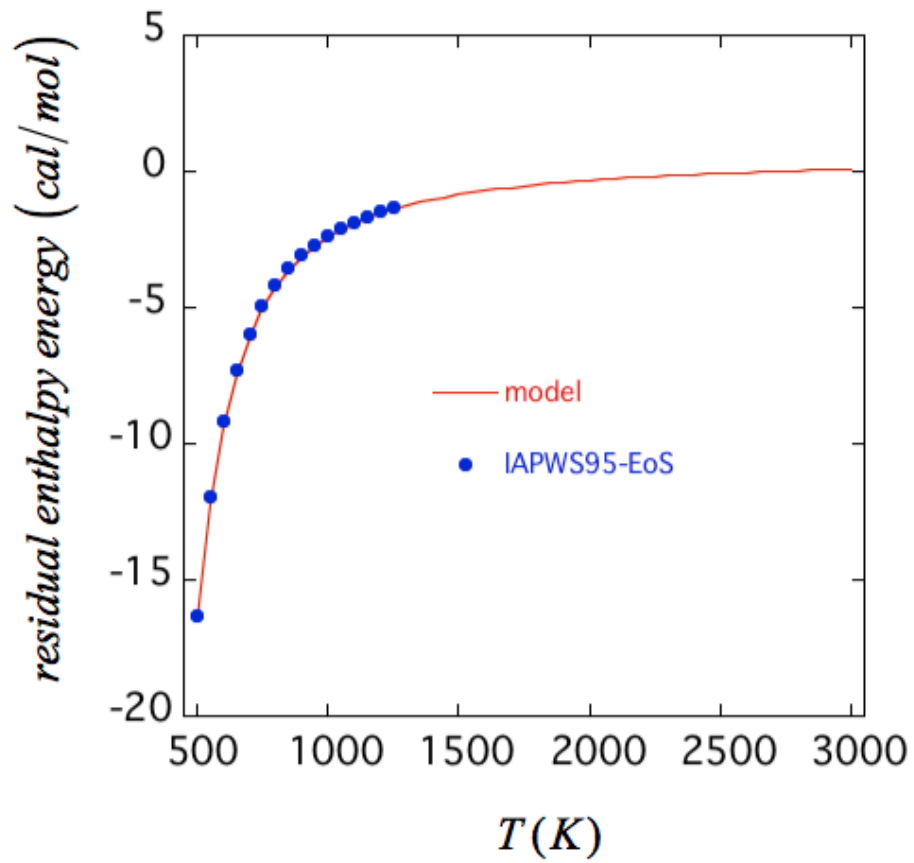


Figure 7

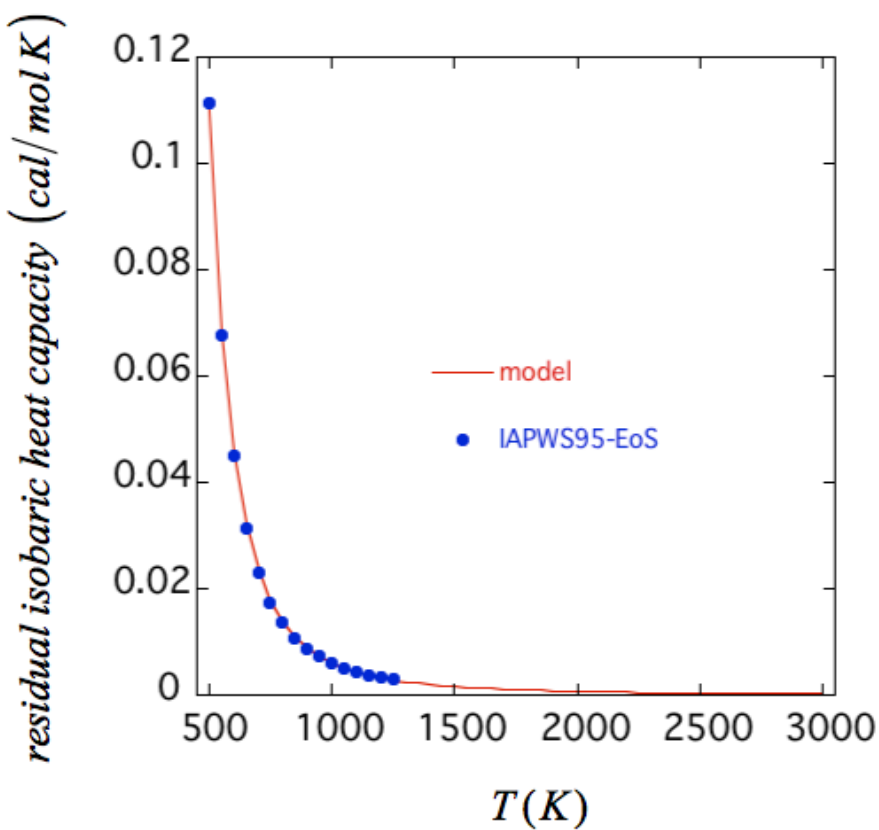


Figure 8

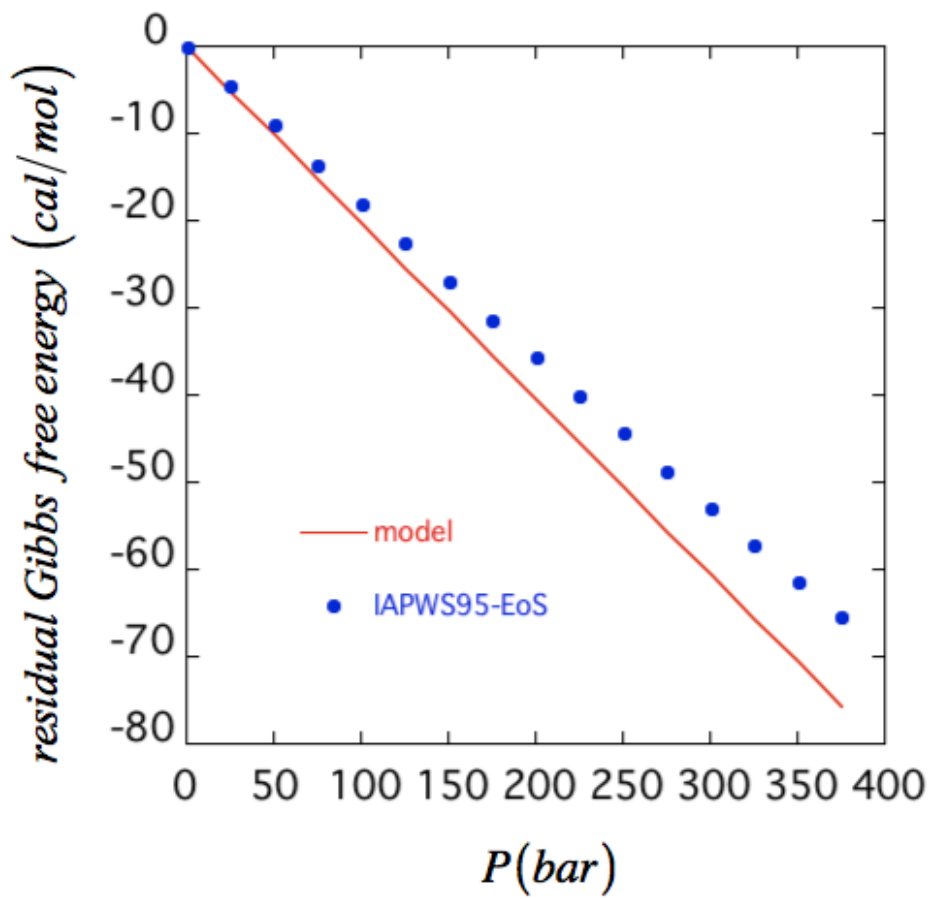


Figure 9

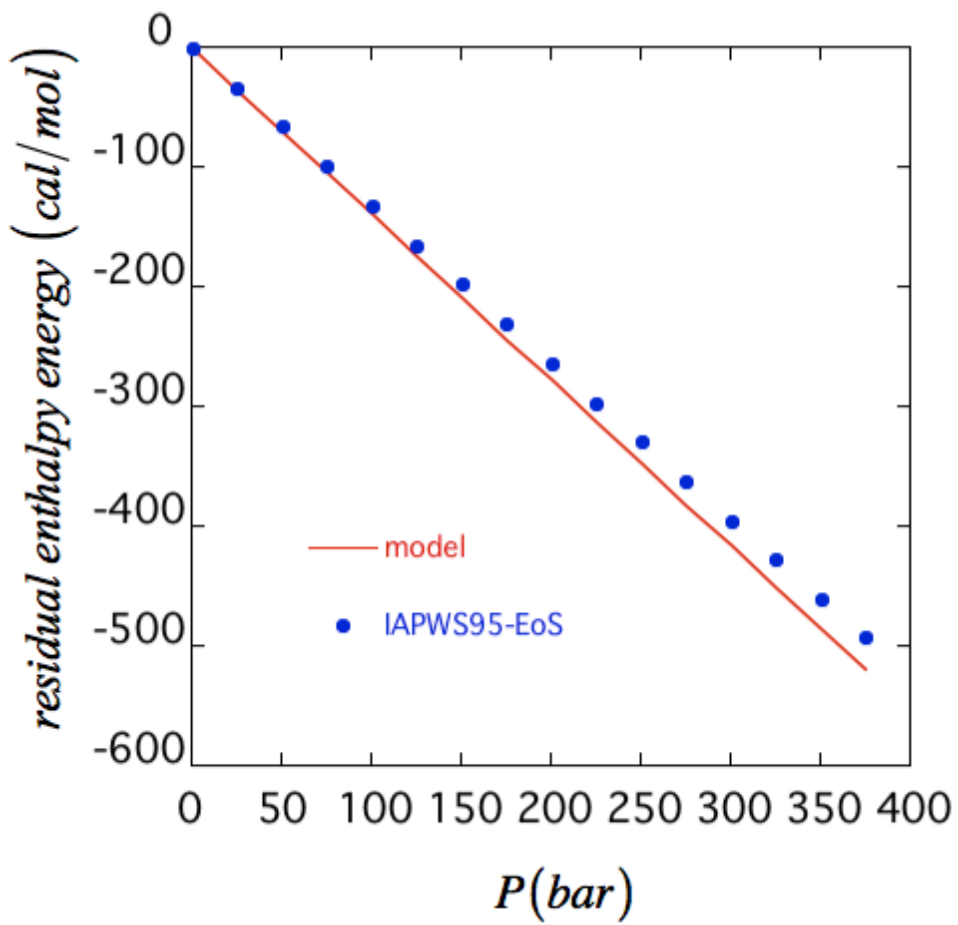


Figure 10

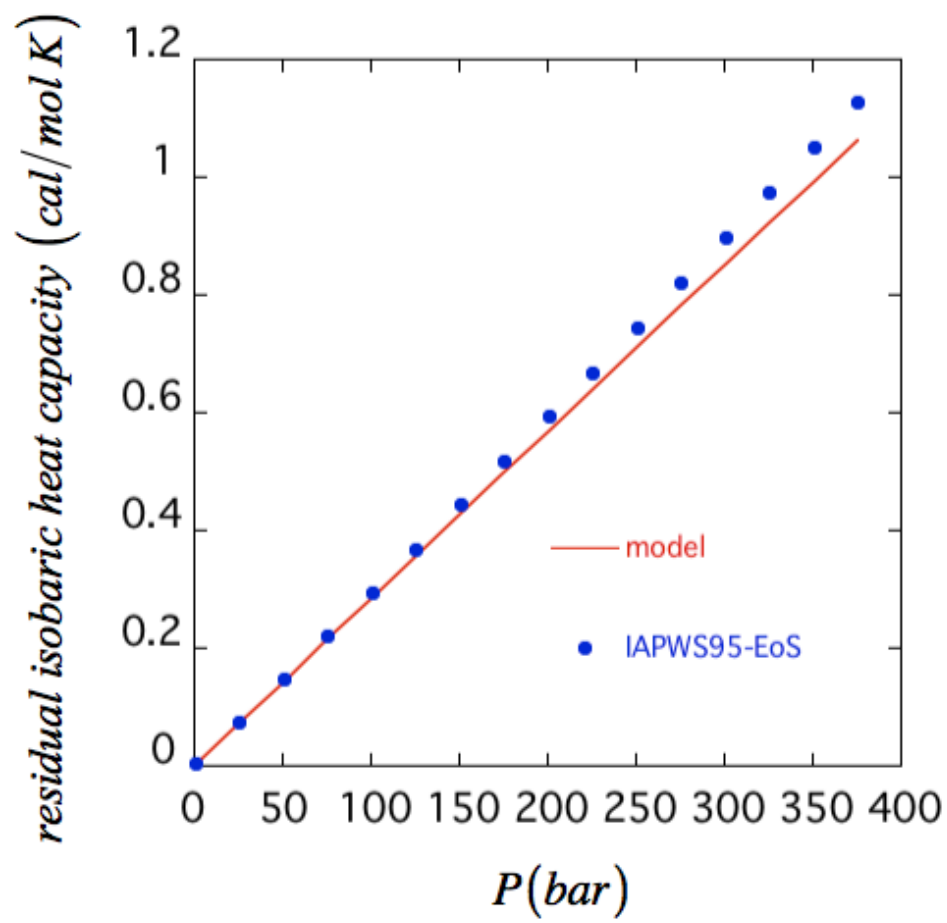


Figure 11

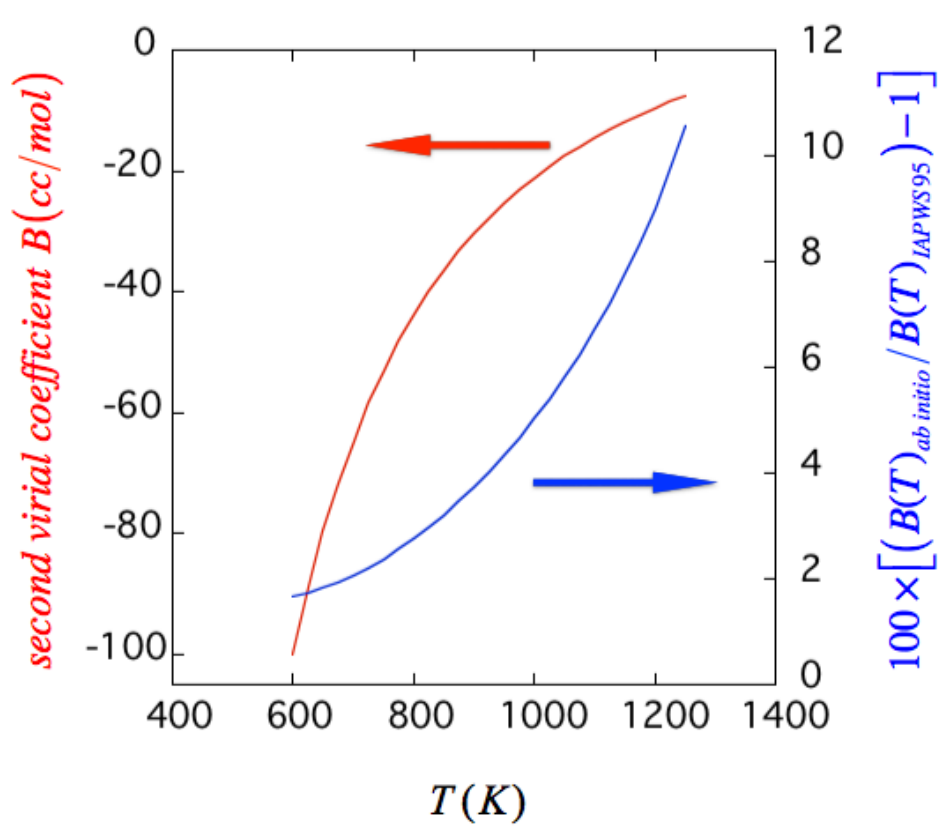


Figure 12

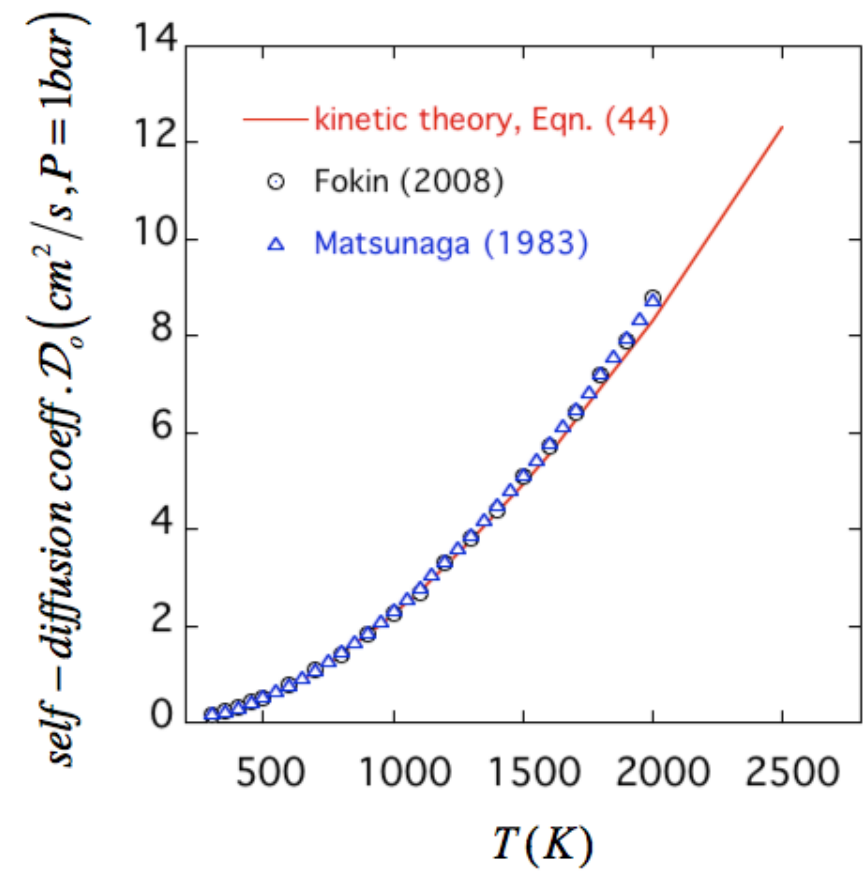


Figure 13

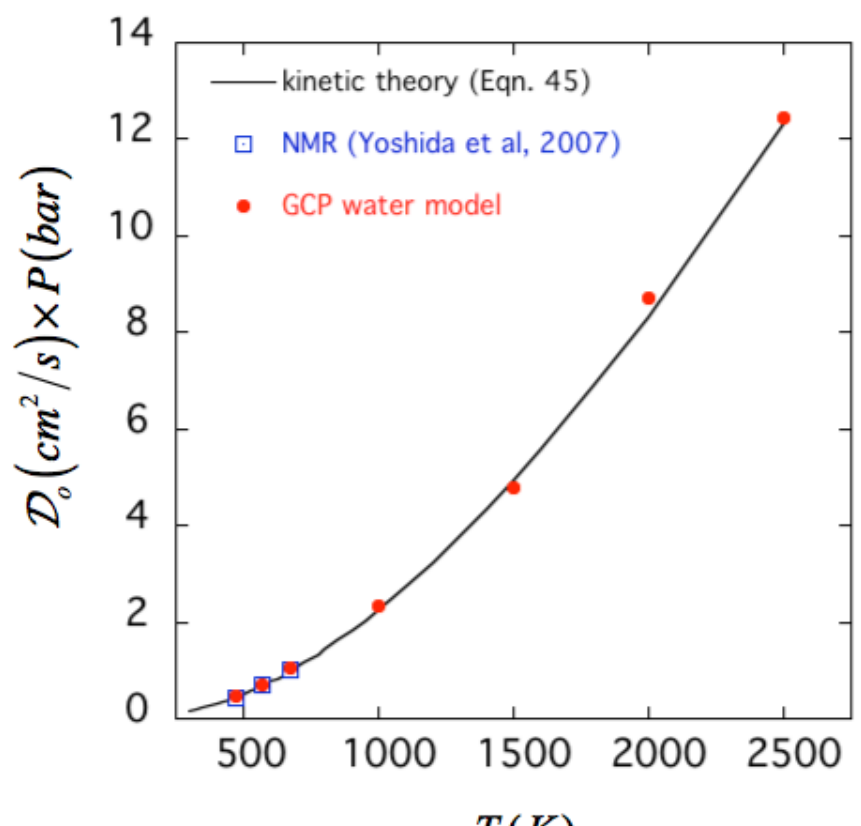


Figure A1

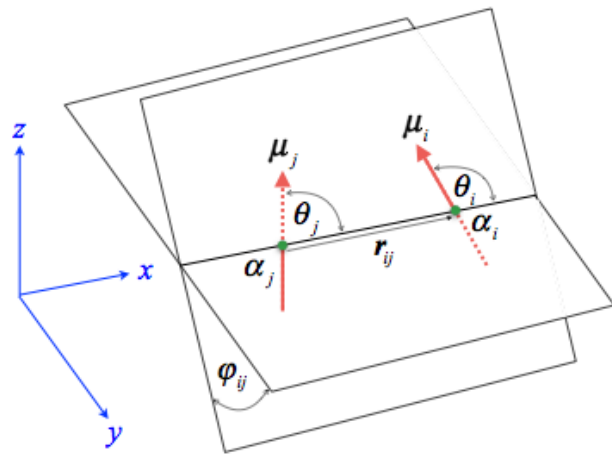


Figure A2

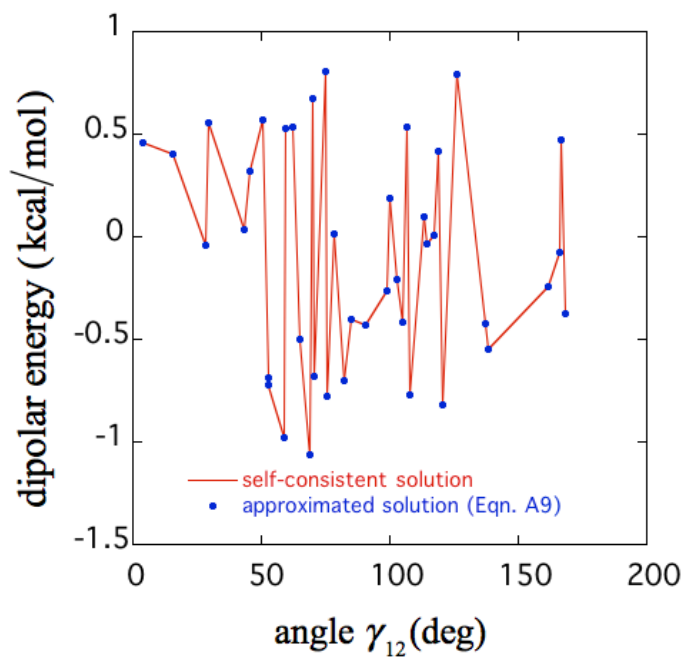


Figure A3

